Mass-Customization of Oral Tablets via the Combination of 3D Printing and Injection Molding

Evert Fuenmayor, Crevan O'Donnell, Noel Gately, Patrick Doran, Declan M. Devine, John G. Lyons, Christopher McConville, Ian Major

PII: S0378-5173(19)30656-8
DOI: https://doi.org/10.1016/j.ijpharm.2019.118611
Reference: IJP 118611

To appear in: *International Journal of Pharmaceutics*

Received Date: 14 May 2019
Revised Date: 16 July 2019
Accepted Date: 10 August 2019

Please cite this article as: E. Fuenmayor, C. O'Donnell, N. Gately, P. Doran, D.M. Devine, J.G. Lyons, C. McConville, I. Major, Mass-Customization of Oral Tablets via the Combination of 3D Printing and Injection Molding, *International Journal of Pharmaceutics* (2019), doi: https://doi.org/10.1016/j.ijpharm.2019.118611

Mass-Customization of Oral Tablets via the Combination of 3D Printing and Injection Molding

Evert Fuenmayor [1], Crevan O'Donnell [1], Noel Gately [1], Patrick Doran [1], Declan M. Devine [1], John G. Lyons [2], Christopher McConville [3] and Ian Major [1]*

[1]Materials Research Institute, Athlone Institute of Technology, Dublin Road, Athlone, Westmeath, Ireland, [2]Faculty of Engineering and Informatics, Athlone Institute of Technology, Dublin Road, Athlone, Westmeath, Ireland, [3]School of Pharmacy, Institute of Clinical Sciences, College of Medical and Dental Sciences, University of Birmingham, UK

***** Corresponding author: Tel.: +353-906-48-3084

Fax: +353-906-42-4493

E-mail: imajor@ait.ie

Short title: Bilayer tablet production via combination manufacturing

Keywords: 3D printing; injection molding; mass-customization; personalized medicine; hot-melt extrusion; bilayer tablets; oral tablets; lovastatin; hydrochlorothiazide.

Abstract

The new frontier of medicine is the personalization of treatment to match a patient's individual needs. Fused-filament fabrication (FFF) offers a platform for the personalization of drug dosage forms, but one of its chief shortcomings compared to other tablet production methods such as dry compression and wet granulation is relatively low throughput. Conversely, injection molding (IM) is a manufacturing technique for the high-volume production of parts, but in which individual part customization is both expensive and slow requiring the modification of expensive mold tooling. Mass-customization is the manufacture of custom products that match the needs of individual consumers but which are produced at the low unit cost associated with high-volume production. We successfully integrated for the first time FFF with IM in a multi-step manufacturing process for the production of custom bilayer tablets loaded with two active pharmaceutical ingredients used in the treatment of cardiovascular disease. The FFF layer was loaded with the diuretic hydrochlorothiazide, while the IM layer was loaded with lovastatin. Infill percentage was varied for the FFF layer as a means to modify drug release. The IM injection pressure was evaluated for its effect on drug release and layer-layer adhesion. The bilayer tablets obtained offered different combinations of drug release profiles, which were governed by a combination of factors, including surface area to volume ratio; IM injection volume penetration into the FFF layer; FFF infill percentage; layer tortuosity and porosity. These different parameters could be utilized to modify the individual release of both drugs from the bilayer tablet. Thus for the first time, we have

demonstrated a viable method for the mass-customization of oral tablets which could hasten the rollout of personalized medicine.

Abbreviations

3D, three-dimensional; 3DP three-dimensional printing; ACN, acetonitrile; API, active pharmaceutical ingredient; CVD, cardiovascular disease; DMA, dynamic mechanical analysis; DSC, differential scanning calorimetry; FFF, fused-filament fabrication; HCTZ, hydrochlorothiazide; HME, hot-melt extrusion; HPLC, high-performance liquid chromatography; IM, injection molding; LOVA, lovastatin; MFI, melt flow index; MFR, melt flow rates; PCL, polycaprolactone; PEO, poly (ethylene oxide); PVP-VA, Kollidon VA64; PM, personalized medicine RPM, revolutions per minute; SD, standard deviation; SDS, Sodium Dodecylsulfate; SEM, scanning electron microscopy.

1. Introduction

The expanding understanding of genomics, in addition to the influence of socioeconomic and biological factors in therapy efficiency, are creating pressure on pharmaceutical industries and regulators for the personalisation of medicine (Aquino et al., 2018). One of the most promising tools to enable personalized medicine is the advanced manufacturing technologies for the fabrication of dosage forms. 3D printing (3DP) is considered to be at the forefront of these technologies (Hamburg and Collins, 2010) as such processes offer the pharmaceutical industry on-demand manufacturing; complex geometries; and enhanced drug release profiles (Goyanes et al., 2014a; Norman et al., 2017; Sun and Soh, 2015; Ventola, 2014). Fused-filament fabrication (FFF) is a 3DP process that has been extensively investigated for pharmaceutical applications with numerous publications highlighting the possibilities the technique affords (Aho et al., 2019; Alhnan et al., 2016; Bansal et al., 2018; Fuenmayor et al., 2018; Healy et al., 2018; Joo et al., 2019; Jonathan and Karim, 2016; Kanger et al., 2017; Okwuosa et al., 2016; Prasad et al., 2019; Quinn, 2018; Ravi et al., 2017; Skowyra et al., 2015; Tidau et al., 2019). The growth of FFF is due to its portability; low-cost capital investment; ease-of-operation; precision; and the ability to produce a wide range of pharmaceutical devices (Araújo et al., 2019; Goyanes et al., 2015c, 2015a; Lim et al., 2016; Melchels et al., 2012; Sadia et al., 2018a, 2018b; Saviano et al., 2019). FFF involves the extrusion of a thermoplastic filament feedstock through a heated nozzle onto a heated print-bed surface. Parts are built in a layer-by-layer manner. It is possible to use more than one material for the same part, and tens of thermoplastic materials are suitable for the process (Fuenmayor et al., 2018). However, FFF is unable to replace current tablet production methods that are capable of the manufacture of millions of tablets per hour, and the pharmaceutical industry is reluctant to switch to a production method with low production output regardless of the involved economic and health benefits (Aquino et al., 2018).

Methods and strategies to improve the scalability of the process must be established to enable adoption of the technology so that the potential benefits – personalization of therapies - can be realized.

Injection molding (IM) is a hot-melt processing technique capable of achieving high-production speeds in a continuous solvent-free fashion with six-sigma part dimensional accuracy. The process is garnering interest for the production of pharmaceutical products (Fuenmayor et al., 2019; Major et al., 2016; Quinten et al., 2009; Zema et al., 2012). In short, the process injects molten formulation into a mold cavity which holds the desired geometry for the finished part. Once the formulation has cooled, the mold opens, and the solid part is ejected before the mold closes, starting the cycle again (Alfreda Campo, 2006). IM as a production method offers advantages when compared to traditional tableting methods, as it is usually preceded by hot-melt extrusion (HME). Thus it is possible to increase the solubility of the drug by creating solid amorphous dispersions (Melocchi et al., 2015). By changing the formulation and the mold shape cavity, it is possible to modify drug release from tablets and capsules produced via IM (Klose et al., 2008; Siepmann and Peppas, 2012). However, this process strategy involves machine down times, extra tooling, and it is not suitable for rapid tailoring of solid dosage forms in comparison to FFF capabilities.

The main objective of this study was to develop a manufacturing platform to overcome the primary limitation of the FFF process, low-production volume. Mass-customization is a production concept in other industries focused on fabricating individually designed products for the consumer while preserving the low-cost derived by the economies of scale provided through mass-production (Da Silveira et al., 2001). By utilizing this manufacturing concept, bilayer tablets were manufactured with customizable drug release profiles using a novel

combination of FFF and IM. There are associated benefits to treating cardiovascular disease (CVD) using multilayered tablets as a therapeutic strategy (Naderi et al., 2012; Simpson, 2006); with this in mind hydrochlorothiazide (HCTZ) and lovastatin (LOVA) were chosen as model drugs as both are used to treat underlying symptoms of CVD (Khaled et al., 2015). The same polymeric formulation was used for both layers, building on our previous work (Fuenmayor et al., 2019, 2018). Nine different tablet batches were created by combining different FFF infill percentages and IM injection pressures, and these batches were tested for dimensional accuracy, weight variation, friability, hardness, surface morphology, interphase adhesion strength, inner physical structure, thermal and melt-flow properties and drug release kinetics. Lastly, the process parameters modifying drug release of these unique tablets were explored.

2. Materials and Methods

2.1. Materials

Polycaprolactone (PCL) in powder form (Capa 6506, average Mw=50,000) was obtained from Perstop (Cheshire, UK). Kollidon® VA64 (PVP-VA) was purchased from BASF Ireland (Cork, Ireland). Poly (ethylene oxide) (PEO) (average Mw=300,000) in powder form was obtained from Sigma-Aldrich (Arklow, Ireland). Both drugs, lovastatin (LOVA) and hydrochlorothiazide (HCTZ), were purchased from TCI chemicals (Tokyo Chemical Industry UK Ltd, Oxford, UK). Sodium Dodecylsulfate (SDS) was purchased from AppliChem (AppliChem GmbH, Ottoweg Darmstadt, Germany). All solvents and reagents were analytical grade. Formulations processed can be found in Table 1

2.2. Hot-Melt Extrusion

All excipients were passed through a 250 µm sieve to obtain equivalent particle sizes and then mixed for 15 minutes at 50 RPM using a Universal Motor Drive 400 (Pharmag GmbH, Hamburg, Germany) attached to a cube mixer. Samples underwent two hot-melt extrusion cycles. The first was to guarantee the homogeneity of the mixtures and second to shape the materials for 3D printing and injection molding applications. A Prism TSE 16 (Thermo Electron, Staffordshire, UK), a benchtop twin extruder, was used for the mixing of the batches; the extruder has two heating zones, barrel and flange, for which the temperatures were 100 °C and 140 °C respectively. The screw speed was 150 RPM, feeding rate 0.6 kg/hr. The machine was equipped with a conveyor belt tilted at 45° with the higher end facing the extruder. The material was air-cooled as it travelled down the belt at a set speed of 80 meters per minute and left overnight for the polymer chains to equilibrate. Filaments were

subsequently granulated using a strand pelletizer SGS 50-E (Reduction Engineering Scheer, Ohio, USA) into 3 mm granules for the second extrusion step.

An MP19TC25 APV Baker 19 mm co-rotating twin-screw extruder (Newcastle-under-Lyme, UK) equipped with a purpose-built filament-forming die was used to shape the materials to serve as feedstock for 3D printing applications. The filament die had a conical shaped cavity, narrowing away from the extruder finishing in a circular orifice (diameter 2.30 mm). The processing parameters were a screw rotation speed of 80 RPM, feeding rate of 1.1 kg/hr and a haul-off speed of 1.4 cm/sec. The machine has a total of 8 heating zones, and from the feeder to the flange the temperature range was 80 °C to 140 °C in 10 °C increments with the last two zones having the same temperature value. The extruded materials were hauled off using a counter-rotating belt haul-off with sufficient speed to maintain a filament diameter of 1.75 ± 0.15 mm necessary for the FFF 3D printing process. Sections of the filament were granulated into 3 mm granules for injection molding.

2.3. Fused-Filament Fabrication

A MakerGear M2 (MakerGear LLC, Beachwood, Ohio, USA) 3D printer was used for the production of FFF inserts. The optimal printing conditions of the blend were determined via preliminary trials and kept constant at: printing speed (500 mm/s), extruder temperature (160 °C), printing bed temperature (55 °C), extruder travel speed (1800 mm/s), number of shells (1), roof and floor thickness (0.2 mm and 0.1 mm), layer height (0.1 mm), infill pattern linear, and the raft and support options turned off. Three different values were chosen for the infill percentage (25 %, 50 %, and 100 %). The 3D design for the tablet was created using SolidWorks® 2014 (Dassault Systèmes, Waltham, USA) and saved as an STL extension format (Figure 1) and dimensions were 1.8 mm in height and a diameter of 10 mm. The STL

file was opened using the monitor and remote control software suite Simplify3D (Cincinnati, Ohio, USA).

2.4 Injection Molding

Injection molding was carried out on a Babyplast® 6/12 (Rambaldi, Italy) equipped with a 14 mm diameter piston. The machine possesses three temperature-controlled areas, plasticising zone, chamber and nozzle and the temperatures were 170 °C, 150 °C and 120 °C respectively. The shot size was determined at a stroke of 13 mm based on the total volume of material necessary per shot to fill all runners, gates and part cavities, the value that was obtained via SolidWorks® plastics flow simulator (Dassault Systèmes, France). The injection molding parameters were optimised for the formulation prior to tablet production. The injection speed was set at 75%, cooling time was 60 seconds, holding pressure was 100 bar, and the mold temperature was 9 °C. FFF tablets were inserted into the mold cavity and pushed until they were touching the back wall of the orifice between injections. Two samples were introduced, one with no drug loading and HCTZ loaded tablets. The floor of the inserts was always facing the injection volume. In Table 2, all tablets fabricated are labelled depending on their combination of production parameters.

2.5 Dynamic Mechanical Analysis

Dynamic mechanical analysis (DMA) was performed on filaments of all formulations using TA Instruments DMA Q800 (Dublin, Ireland). The test was performed in a single cantilever mode using a frequency of 1 Hz and an amplitude of 15 µm. The temperature range between −80 °C to 150 °C with 3 °C/min rate was used to determine the storage modulus, the loss modulus, and the glass transition temperature (tan δ) for all three formulations.

2.5.2. Filament Stiffness

The temperature range −80 °C to 150 °C with 3 °C/min rate was used to determine the stiffness and glass transition temperature (tan δ) for placebo and drug-loaded formulations after each processing step. The test was carried with a constant frequency of 1 Hz and an amplitude of 15 µm using the single cantilever mode.

Stiffness is calculated as load divided by deformation. Where the load is determined as the force applied to the material in any given moment to obtain the desired amplitude expressed in Newtons (N). Deformation is the distance the sample has moved from its original position at the beginning of the test, and it is expressed in meters (m).

2.5.3. Filament Brittleness

The calculation of filament brittleness involved two discrete tests, which were performed on 25 mm filament lengths of all formulations using a TA Instruments DMA Q800 (Dublin, Ireland). Storage modulus (E′) values were taken in single cantilever mode at room temperature with a frequency of 1 Hz. Cylindrical samples had a length of 17.5 mm and varying diameters. The test was performed in triplicate. Quasi-static 3-point bending of 25 mm filament lengths was performed separately on the Q800. The force applied to the samples was ramped up at 3 N/minute, and the test was stopped when samples broke, or a maximum displacement was achieved. The Brostow-Hagg Lobland-Narkis Equation (Equation (1)) for brittleness was used to obtain brittleness (B) values (Brostow et al., 2006). In the equation, E′ is the DMA storage modulus at 1.0 Hz at room temperature and strain-at-break (%), εb is calculated from room temperature 3-point bending.

2.6. Melt Flow Indexing

The melt flow rates (MFR) were measured using a Zwick Roell Cflow extrusion plastometer with a 2 mm orifice die. All testing was performed with a fixed weight of 2.16 kg following

the guidelines of the ASTM standard D1238-13. The temperature range for the test started at 110 °C and increased in jumps of 10 °C. The test was stopped once the drop in viscosity of the tested materials did not allow for the completion of the experiment.

2.7. Differential Scanning Calorimetry

Differential scanning calorimetry (DSC) was employed for thermal characterization of material blends and fabricated tablets, using a TA Instruments DSC 2920 Differential Scanning Calorimeter (Dublin, Ireland). Samples weighed between 8 – 12 mg and were placed in non-hermetical aluminium pans, which were crimped prior to testing with an empty crimped aluminium pan for reference. Each sample was summited to a heating cycle to remove thermal history consisting of a ramp from room temperature to 210 °C at a rate of 10 °C/min for samples containing LOVA and 300 °C for placebo and HTCZ containing samples. The maximum temperatures of this first cycle were determined based on the melting point of drugs (LOVA Tm: 174.5 °C and HCTZ Tm: 274 °C) to prevent heat-associated degradation. This was followed by a cooling cycle down to 0 °C at a rate of 5 °C/min. Data recording was activated, and the temperature was ramped at a rate of 10 °C/min until 300 °C was reached.

2.8 Scanning Electron Microscopy

Scanning electron microscopy (SEM) was performed on a Mira SEM (Tescan Oxford Instruments, UK) using a range of magnifications to evaluate the surface morphology of the tablets and drug using the secondary electrons function. Tablets with or without drug were snap broken through the transversal plane and cross-sectional areas examined under the microscope. Prior to imaging, Samples were placed on an aluminium stub and were gold coated using Baltec SCD 005 sputter coater (BAL-TEC GmbH, Germany) for 110 sec at 0.1 mBar vacuum before observation.

2.9. Tablet Hardness

Each placebo formulation underwent tablet hardness testing according to USP <1217> using a Schleuniger Pharmatron Model 6D Tablet Tester (Solothurn, Switzerland). The tablets were selected at random with each tablet being placed into the hardness tester, and the maximum force-to-break (Newton) was measured.

2.10. Tablet Friability

In order to determine the physical integrity of tablets, an auto-friability tester PTF E/ER (Pharma Test Apparatebau GmbH, Hainburg, Germany) was utilised. Following the USP standard 32-NF 27, tablets were laid in a sieve and using a soft brush; any dust was removed from them. Then tablets were weighed until their combined weight was equal or greater than 6.5 g and introduced into a drum rotated at a speed of 25 ± 1 RPM for 4 min. Tablets were removed and brushed again to remove any dust and reweighed.

2.11. Tablet Layer Adhesion Test.

Measurement of the tablet interfacial adhesion was based on the work of Busignies *et al.* (Busignies et al., 2014). An aluminium base with an indentation was used to hold the tablets in place with their lateral surface facing upwards. A Lloyd LRX Universal tester (Lloyd Instruments Ltd, Bognor Regis, England) equipped with a force transducer capable of registering force changes of 0.01 Newtons was used. The machine was equipped with an attachment that would deliver a piercing force in the divisor line between the tablet's layers. The force exertion rate was controlled using the movement speed of the punch,

which was 0.05 mm/min and the test was automatically stopped once a fracture extended through the sample. A total of 5 tablets per batch were used for this test.

2.12. Drug Release Studies

Dissolution testing of tablets (n = 3) was performed on Distek dissolution system 2100B with a Distek temperature control system TCS 0200B (Distek Inc., USA) according to USP Dissolution Apparatus I. The dissolution media (900 mL per vessel) was deionized water and 1% w/v SDS (AppliChem GmbH, Ottoweg Darmstadt, Germany) and the temperature was 37 ± 0.5°C. The stir rate being 50 RPM and the basket mode was used. At predetermined time intervals, 5 mL was withdrawn from each vessel and replaced with pre-heated media. The withdrawn samples were filtered through 0.45 µm filter, and high-performance chromatography was used to determine the amount of drug released over time. The dissolution profile was observed from a plot of time versus area under the detection peak.

2.12. Drug release quantification

High-performance liquid chromatography (HPLC) was used to determine the drug release over time of LOVA and HCTZ. The HPLC equipment was a Waters 2695 Separation Module equipped with column and sample temperature controls which was connected to a Waters 2487 Dual Absorbance Detector. The samples and column were kept at 37 °C for the duration of the tests, and the detector was set at 238nm and 271nm corresponding to the λmax for drugs used in this study. The data were collected and integrated using Empower® Version 2.0 software. The column was a Luna C18(2), 5 µM, 150 x 4.6 mm, equipped with a precolumn Security Guard Cartridge C18, 4.0 x 3.0 mm, (Phenomenex Inc., UK). Three lines were used for the pumping of solvents, and two methods were developed to detect both drugs reliably. A was Acetonitrile, B was deionized water, and C was a solution of Acetronitrile

with 0.1% (v/v) trifluoroacetic acid The injection method was a gradient consisting of pumping solvents A and B at a ratio of 50:50 for the first 4 minutes; at this time point the proportion was changed to 80:20 for the following 6 minutes when the ratio was switched back to 50:50. The second method pumped lines B and C in a ratio of 5:95 and was used for purging the injection line from built up of SDS. The flow rate was kept constant for both methods at 1 ml/min, and the injection volume was 10 µl.

2.13. Statistical Analysis

Data handling and analysis were performed using GraphPad Prism 5 (GraphPad Software Inc., UK). Test data was input into the software, and mean, and standard deviation values were calculated for replicate sets of data. The significance threshold was set at 0.05. Error bars represent standard deviation unless otherwise specified in the figure caption. The mean values are presented in the figures in the results section. Multiple comparisons among subgroups were performed using a Bonferroni posthoc test to differentiate drug release curves.

3. Results and Discussion

3.1 Mass-customization of tablets

A mass-customisation manufacturing strategy requires breaking down complex product designs and process operations into smaller, discrete subassemblies to provide consumers with tailored products at affordable prices (Alford et al., 2000; Deradjat et al., 2017). In the context of this research, the complex product is a tailored tablet with well-defined therapeutic properties based on the needs of individual patients or population sub-groups but fabricated at efficient production rates in a reliable, predictable and sustainable manner. We propose the mass-customisation of solid dosage forms by combining the highly modifiable but slow process of FFF with that of IM, which offers high-volume manufacturing but little customisation. In our model, several offline FFF printers would manufacture tablet inserts that would provide all the required tailored drug release profiles. While the injection molding stage is designed to fabricate the majority of the tablet; the bulk of the tablet that is appropriate to all patients (dose, drug, etc.). Based on a required therapeutic profile, printed inserts would be fabricated to provide the additional dosage, drug and/or to determine the final release profile. The inserts would then be sent to the injection molding station for insertion into an IM mold tool, where the remaining bulk of the tablet would be finalised in minutes. Various types of inserts (different release profiles or drugs) can be molded on the same injection molding station. Figure 2 depicts a flow chart of the envisioned industrial setting for the manufacturing of tablets, applying the concept of mass-customisation.

In our laboratory setting, FFF 3D printing of a batch of thirty full tablets would take 240 minutes. Each injection molding cycle to fabricate two tablets took 90 seconds. Thus, thirty tablets took 22.5 minutes to produce. Our combined approach required 120 minutes to FFF 3D print thirty tablet inserts plus 22.5 minutes of injection molding. Combined time,

therefore, was 142.5 minutes. Considerable time savings could have been made by molding more than two tablets per cycle by adding more tablet cavities and utilising more than one printer at a time. In industrial practice, 3D printing would still be the rate-determining step but would be offline, and the batches of inserts made ahead of the scheduled molding stage; ideally made for stock. Robotics would be implemented to bridge the two processes allowing for full process automation, thus removing operator errors and increasing the continuity of the manufacturing process.

3.2 Manufacturing observations

3.2.1 Hot-melt extrusion and characterization of filaments

Hot-melt extrusion compounding of the three formulations described in Table 1 was successful with no visibly observable degradation of the materials. The first melt compounding of the formulations improved the homogenous mixing of the drug in the polymer matrix. The twin-screw extruder employed in this processing step was equipped with a set of modular twin screws with three kneading areas which increases the dispersive mixing properties of the process (Cheng and Manas-Zloczower, 1997; Nakayama et al., 2018) and the higher screw rotational speed during the first processing step has a similar effect on the homogeneity of the formulation (Villmow et al., 2010). The shorter barrel of the machine also reduces the residence time, which decreases the exposure of thermally labile compounds to heat and shear stress, controlling their degradation (Fornes et al., 2003; Radlmaier et al., 2017). Three formulations were extruded, a placebo blend and two drug-loaded formulations (5 % w/w). Lovastatin (LOVA) is a fungal metabolite which is administered in its lactone form and is metabolized in the liver to its active hydroxy-acid form, which makes it less soluble in water when compared with other statins (Mitra et al., 2013). This combined with its high permeability, makes it a BSC Class II drug compound.

Hydrochlorothiazide (HCTZ) is a diuretic drug used to treat high blood pressure and swelling due to fluid build-up and is classified as a BSC Class IV (low solubility/low permeability) drug compound (Ndindayino et al., 2002). The use of melt compounding techniques to increase the solubility of drugs is not new to the literature (Maniruzzaman et al., 2012) and there have been reports for the low bioavailability for these drugs when administered (Barbhaiya et al., 1982; Chen et al., 2010, 2013; Corveleyn and Remon, 1998; Patel et al., 1984; Qureshi et al., 2015; Yadava et al., 2015) making them suitable candidates for HME applications.

The stability and crystal structure of the formulations was evaluated using DSC analysis after the first processing step and can be found in Figure 3 (a). The melting peaks of the drugs and polymers are visible; however, for drug-loaded blends, these drug melting peaks are not present. HCTZ and LOVA melted at 273.5 °C, and 175.3 °C respectively and melting peak for excipients occurred at 62.0 °C as it is expected for a PCL/PEO blend (Fuenmayor et al., 2018) while a relaxation corresponding to PVP-VA appeared around 100.0 °C. The absence of a melting peak for the drugs can be attributed to solubilization of the drug crystals in the polymeric matrix during the HME process (Alshahrani et al., 2015; Fuenmayor et al., 2019; Huang and Dai, 2014; Sarode et al., 2013). Materials were granulated and sieved through a metallic mesh with an aperture of 3 mm, and the process was repeated until all granules were of a uniform size to prevent feed-related surging during the FFF feedstock material manufacturing stages (Frankland, 2011).

A second HME process was used to create a filament suitable for the FFF process. The barrel of the second extruder was longer, and the screw has a configuration resulting in less shear stress being applied to the material as it travels forward to a specially designed nozzle attachment. A more detailed description of the procedure for the fabrication of FFF filament using this formulation is given in previous work (Fuenmayor et al., 2019, 2018). Among

some of our findings was the identification of the narrow range of mechanical properties that determined the suitability of a formulation for FFF applications. DMA was used to compare how the formulation changed after being processed twice in comparison to the single processing step from our earlier work. We used the Brostow-Hagg Lobland-Narkis approach to determine the brittleness of the formulation, and the values are presented in Table 3. A brittleness value of $\leq 2x10^4$ %.Pa is required for a formulation to be suitable for the FFF process (Fuenmayor et al., 2018), and the formulation was below this threshold after two HME processing steps. The reduction in the storage modulus (157.97 Pa) is believed to be a consequence of the two-step HME process creating polymer chain scissions and reducing the polymer molecular weight (González-González et al., 1998). Materials during the HME process undergo thermal and mechanical stresses that can cause degradation of the polymer chains, compromising the performance of the matrix. Degradation was observed in the reduction in dynamic response and strain at break for this particular formulation and experimental conditions between the first and second processing step (Table 3).

Along with brittleness, melt flow is another parameter crucial for efficient FFF printing. This property relates to viscosity, and it is affected by temperature. Wang et al. determined that a formulation must have a minimum flow rate of 10 g/10min for FFF (Wang et al., 2018). The incorporation of the two drugs had different effects on the formulation. LOVA had a plasticizing effect, increasing the flow of material over the temperature range, while HCTZ had the opposite effect (Figure 3 (c)) Reprocessing the samples did not have any apparent effect on the thermal properties of the samples as shown in Figure 3 (b), all transition peaks remained with no noticeable shift when compared to Figure 3 (a).

DMA temperature sweeps were utilised to evaluate the mechanical performance of the samples along with thermal events and miscibility of ingredients (Fuenmayor et al., 2018). Figure 4 shows the DMA analysis of drug-free and drug-loaded samples (n=3). HCTZ

(Figure 4 (c)) had little effect on the formulation when compared to the thermogram for drug-free in Figure 4 (a). However, there was the postponing of sample yielding for HCTZ loaded specimens. DMA can only be performed on samples before the onset of softness (Menard, 1999). The extended test temperature range for the samples loaded with HCTZ could be interpreted as an increase in heat deflection temperature (Menard and Menard, 2015) which correlates with the observed melt flow behaviour during the MFI test.

3.2.2 Fabrication of tablets.

The polymeric matrix chosen for this body of work has been used in our previous publication to directly compare tablets fabricated via direct compression, IM and FFF (Fuenmayor et al., 2019). During this previous study, the effects of three FFF parameters (infill percentage, infill pattern and layer height) on 3DP tablets physical and pharmaceutical properties were elucidated. The main differences between tablets fabricated using these three processes were also laid out. It was sensible to keep the formulation constant since it has been characterised in-depth and this would allow to better attribute the behaviour observed from the tablets to the manufacturing processes.

HCTZ is administered in immediate-release formulations once or twice daily, and the drug half-life is 12 – 24 hrs when administered orally (Herman and Bashir, 2019). LOVA shows promising enhanced health benefits when administered in an extended-release fashion (Curran and Goa, 2003). When combining this information with our previous experience on drug delivery from IM and FFF tablets (Fuenmayor et al., 2019), it was sensible to use the model drug HCTZ in the 3D printed layer since it offers a faster release when compared to IM parts of the same volume. Following this rationale, LOVA was chosen as the model drug for the IM layer. Two processing parameters were evaluated for their effects on drug release without modifying tablet volume and geometry. FFF infill percentage changes the exposed

surface area, porosity and permeability of the tablet (Konta et al., 2017; Palo et al., 2017; Yu et al., 2008), while IM injection pressure modifies the tortuosity of the polymer molecular chains and matrix porosity (Quinten et al., 2009; T Quinten et al., 2011). The fabrication of tablets was performed in sequential stages of manufacture. Firstly the HCTZ loaded substrates were fabricated via FFF and inserted into the mold cavity of the tablet mold tooling. The LOVA loaded formulation was then injected into the tool in a molten state and allowed to cool, thus forming a bilayer tablet.

Filaments loaded with HCTZ with a diameter of 1.75mm ± 0.1mm were destined for the fabrication of FFF substrates. The printing parameters were initially the same as our previous work (Fuenmayor et al., 2019, 2018), but when the drugs were added flow from the nozzle was poor. Therefore, the hot-nozzle temperature was increased to 160 °C and the consistency of the deposited layers improved, probably as a consequence of exceeding the 10g/10min melt flow rate threshold (Wang et al., 2018). Tablets were fabricated using three different infill percentages (25, 50 and 100 %). The floor of 3D printed parts was in contact with a heated surface of the printing bed that increases the adhesion of the part to the printed surface by relaxing the polymer. Although beneficial to the success of FFF projects, this feature of the FFF process created disparities in the surface finish in the printed tablet layer. Hence the rationale behind purposely facing the top of the 3D printed layer in the injection direction to allow for the penetration of the molten material into the void volume to promote layer-layer adhesion (Busignies et al., 2013; Castrati et al., 2016).

3.3 Physical Characterization of bilayer tablets

Tablets were fabricated successfully as outlined. One of the first noticeable features of the tablets was the ingress of the injection volume in and around the 3D substrate. In Figure 5 (c) and (d) an overmolding event is observable, resulting from small dimensional deviations of

the 3D inserts which allow for the injection melt volume to engulf the insert. This effect was further aggravated by increasing injection pressure and any dimensional inaccuracy of the inserts (Figure 5 (e) to (g)). From left-to-right, the samples were manufactured using a decreasing amount of pressure while all inserts were the same, and the parting line between substrate and injection volume is more noticeable.

To understand the degree to melt penetration, the cross-sectional area of bilayer tablets were examined via SEM imaging and are shown in Figure 5 (h) to (p). The FFF printed patterns are clearly distinguishable in one-half of the tablets; however, there seems to be a direct correlation between injection pressure and injection volume penetration. Figure 5 (n) to (p) shows that the melt penetration volume on injection tended to overmold instead of penetrating the 100% infill FFF tablet layer insert. Also, the higher the injection pressure, the greater the degree of overmolding.

The adhesion properties at the bilayer are shown in Figure 6. The breaking force between layers was selected as the highest value, and the displacement represents the distance of vertical penetration before failure. These values are presented in Table 4. The greatest deviation for forces and displacement are seen for tablets fabricated using 25 % infill. The trend is not linear, and the forces observed are more consistent for tablets with 50 % infill when compared to 100 %. For the displacement, the opposite finding was observed. We hypothesize that the lower infill allows for greater penetration of molten polymer during the injection cycle, as seen in Figure 5 (h) to (j). The level of penetration is visually more prominent for these tablets when compared to those depicted in Figure 5 (k) to (p). The higher and more stable breaking force for batches 4 to 6 (Figure 5 (k) to (m)) could also be explained by this phenomenon, a more compact internal structure for the 3D inserts will increase the tablets' mechanical integrity (Kanger et al., 2017) in combination with a degree of melt penetration. For batches 7 to 9, melt volume penetration was impossible due to the

absence of void spaces with a 100 % infill (Figure 5 (n) to (p)), and some overmolding was present. This lack of penetration explains the smaller total displacements for these tablets but also the smaller forces when compared to batches 4 to 6. Batch 7 could be considered an outlier for its higher breaking force, and larger sample size should be analyzed to confirm this.

The mechanical properties of the tablets were all more than 460 N, which is the limit of the test machine with little or no deformation and no breaking. The mass of FFF layers increased with infill percentage as to be expected (data not shown), and the average mass for all batches was 348.84 mg (Standard deviation: 10.94 mg).

3.4 Drug dissolution.

One of the obstacles of working with a combination drug product is the possible interactions between the active or excipient components of the formulation. The solubility of drugs was expected to be increased via HME. The selected media for our previous work was 0.2 M hydrochloric acid, pH 1.2 at 37 ± 0.5 °C (Fuenmayor et al., 2019, 2018) and we attempted to continue using this fasten stomach conditions for the drug release studies described herein. One complication is that LOVA is administered in its lactone form and goes through acidic hydrolysis in the stomach, turning into LOVA acid and further into its methyl ester form (Huang et al., 2010). Since these would hinder the quantification of the release rate of the drug from samples, we decided to use purified water and surfactant in concentrations determined via preliminary screening trials to have a clear picture of LOVA's release rate. Using UV spectroscopy and stock solutions of solvent, dissolution media and drugs, it was determined that HCTZ would hinder the detection of LOVA when both drugs are suspended in the same media (data not shown).

The equipment available allowed for the dual UV-wavelength method, and the detector was set at 238 nm and 271 nm. The selected solvent gradient, injection and flow rate were fine-tuned during preliminary stages, and we successfully managed to reduce HPLC injection times from 35 minutes to 11 minutes. Standard solutions of LOVA and HCTZ and a combination of both drugs were analysed to determine any interactions and compare the detection capabilities to the runs of the drugs alone. The R-square value for LOVA at the wavelength 238 nm was 0.98, and the same result was obtained for HCTZ at 271 nm.

In Figure 7, the release for both drugs over 72 hours is depicted. We successfully quantified over 50 % of the drug in the media for both drugs and all batches except LOVA in batch 9. One of the first noticeable aspects in Figure 7 is that both drugs had different release ranges. HCTZ was contained to a smaller range than LOVA, similar to those expected for 3D printed tablets (Fuenmayor et al., 2019; Goyanes et al., 2015d, 2014b; Prasad and Smyth, 2016). Whereas the influence of injection molding parameters was not as documented in the literature in comparison (Loreti et al., 2014; Quinten et al., 2011), and to the best of our knowledge injection pressure has not been evaluated before in this context.

In an effort to simplify the data and illustrate better the effects of the process parameters on drug dissolution, we calculated the average release based on infill percentage and injection pressure, and the results can be found in Figure 8. HCTZ behaves accordingly as reported in the literature up to 24 hours, with the increasing infill delaying the release rate of drug (Fuenmayor et al., 2019; Goyanes et al., 2014a) and 50 % infill substrates surpassing those manufactured using 25 % in terms of drug release at the 24 hours mark. This effect is believed to be a consequence of injection melt penetration, acting as a permeating barrier deferring media penetration. This phenomenon was also at play for batches 1, 2 and 3 based on the slower release rate observed when compared to 3DP tablets fabricated using the same printing parameters and formulation (Fuenmayor et al., 2019). All substrates released over 40

% of their drug content after 24 hours, but a different trend occurs after this time point. After two days, HCTZ release began to slow for the 25 % infill due to the highest level of injection volume penetration, which created a barrier for the dissolution media. At 48 hours the detected quantities of the drug were 64%, 73% and 82% for 100%, 25% and 50% infill substrates respectively, and these drug quantities reached 100%, 89% and 78% after 72 hours of testing.

Injection pressure offered two different drug release profiles, a slower release for tablets fabricating using the lowest pressure and a more sustained release for 60 and 120 bar. A Two way ANOVA of these two latter curves showed no significant differences in the drug release values ($P > 0.05$ at all time points). Tortuosity will affect the drug diffusion properties of the polymer matrix directly (Chien, 2007), and in return the tortuosity can be increased by higher processing temperatures and compaction force (Crowley et al., 2004) and porosity of the matrix will also be decreased in relation to an increase in tortuosity (Young et al., 2002). Our initial intent was to control this matrix property using injection pressure and document the extent of this phenomenon. However, the results suggest that other events are modifying drug release for both drugs from the bilayer tablet. Total tablet volume, injection melt penetration and FFF infill percentage all combine to control drug release from the bilayer tablets. SEM images of tablets show a difference of inner structure, and cross-sectional area as a consequence of both FFF infill percentage and IM injection pressure interactions and these changes are responsible for the observed drug release profiles due to changes in the surface area to volume of the substrates. It has been previously demonstrated that (i) tablets with a higher aspect ratio (height-to-radius) had faster release rates and that (ii) for tablets with different volume, those smaller will exhibit faster dissolution rates because of their higher surface area to volume ratio (Goyanes et al., 2015a; Martinez et al., 2018; Reynolds et al., 2002).

Tablets fabricated using an injection pressure of 20 bar had the slowest release rate for LOVA, and they follow a similar trend at different drug dissolution rates, with a steady release up to 48 hours followed by a burst in drug release. Batch 4 was the slowest for the first 48 hours, releasing 19 % of its drug content over 48 hours and 68 % overall at the end of the test. Batch 1 and 7 behaved similarly for the first 48 hours (24 % and 29 % respectively), and batch 7 was the only set to surpass the 70 % drug release mark (76 % after 72 hours). Batch 1 released 58 % and batch 4 68% at the same time point. HCTZ substrates released over 95 % of their content after 72 hours, and the drug quantity rate followed the order 100 % infill > 25 % infill > 50 % infill. The delayed-release observed for tablets fabricated with 25 % infill is believed to be a consequence of infill collapse and injection melt volume acting as a permeation barrier for the media, as it will present easier penetration for the melt during the injection step as it can be observed in Figure 9 (a) to Figure 9 (c) when compared to Figure 9 (d) to Figure 9 (f).

An increase in the injection pressure resulted in the fastest release for LOVA (Figure 10). Applying an injection pressure of 60 bar accelerated the drug release to a steadier dissolution over time. Batch 5 was the fastest during the first 48 hours of testing, releasing a little over half its content after a day and over two thirds after two days, finishing with 90 % of its drug content left. Batch 2 had the highest release overall, a 99 % drug released over three days, and at time points 24 and 48 hours drug quantities are 40 % and 67 % respectively, in contrast, batch 8 had 34 % and 59 % of its drug content released at the same time points concluding with a total drug release of 88 %. A similar trend for HCTZ substrates was noticeable when comparing tablets made using 60 and 20 bar. 100 % infill had the slowest release rate after 72 hours (74 %) followed by 25 % infill (84 %) whereas substrates fabricated using 50 % infill had all of drug content released at this time point. Batch 2 released 60 % of its content after

24 hours compared to 55 % and 39 % for batches 5 and 8. The drug release rate slowed down, and after 48 hours, batch 5 overtakes batch 2 in total drug released sitting at 79 %.

In contrast, batch 2 and batch 8 had dissolved 75 % and 65 % of their content after two days. The opposite effect for LOVA for batches 2 and 5 was observed, and it is assumed that the same mechanisms explained above are acting over these tablets for both LOVA and HCTZ. A higher force resulted in slower release rates for HCTZ for batch 2, 5 and 8 if compared to batch 1, 4 and 7 due to a combination of increased tortuosity and smaller surface area (substrate) due to the higher area covered by the injection volume at higher injection pressures.

The highest injection force used in this study displays a similar tendency in the order of drug released over time (Figure 11). Batch 6 sits highest for LOVA release at all time points of the test, with batch 3 behaving somewhat similarly to batch 1 and 2 for the same drug with a slow-release for the first 48 hours ending in a rapid release between this time point and the end of the test. As for batch 9 LOVA, the drug release rate was the slowest in this whole project, with an average of 13 %, 29 % and 46 % release after 24, 48 and 72 hours respectively. As for the drug-loaded 3D printed inserts, HCTZ was released following a tendency of increases in infill percentages delaying drug release (Fuenmayor et al., 2019) but the differences between batches 3 and 6 in drug release over time are non-significant, and the same can be said for batch 9 up to 48 hours ($P > 0.05$). All substrates release at least half of their content after one day. Batch 3 released 60 % and 72 % drug release after 24 and 48 hours. In comparison, batch 6 averaged 51 % and 66 % while batch 9 had 48 % and 65 % of its drug content for the same time points. After 72 hours, the released drug were 96 %, 95 % and 74 % for HCTZ in batches 3, 6 and 9 respectively.

It is hypothesised that the injection volume distribution holds the explanation for the observed drug release profiles. SEM of the cross-sectional area of tablets shows that for samples with 50 % infill ((d), (e) and (f) in Figure 9 to Figure 11), the injection volume tended to cover the outer surface of the substrate, whereas the samples 25 % infill ((a), (b) and (c) in Figure 9 to Figure 11), the volume penetrated closer to the core covering a greater area. Therefore, the the dissolution media will be in contact with a greater surface area for LOVA for batches with higher infill at the beginning of the test, explaining the faster release for the first two days and secondly, the height of the cross-sectional area of the tablet is higher for tablets with the lower infill, which results in a higher aspect ratio, thus accelerating release rate once the media reaches the inner core of the tablets (Goyanes et al., 2015b; Siepmann et al., 1999).

4. Conclusions

3D printing of pharmaceutical applications could be one of the key-enabling technologies for the personalization of medicine. However, it is a slow process that cannot compete directly with more established processes for the production of tablets. IM easily matches the high-volume production capabilities of the tabletting industry but modifying drug release, and sample geometry is an expensive and slow process. Mass-customization is currently being explored in manufacturing industries as a means of providing consumers with bespoke products but at the reduced costs associated with high-volume production. The merging of a highly modifiable production method with a rapid, autonomous process would allow for both personalization and high-throughput production, and it was the driving idea behind this body of work. FFF was successfully integrated with IM for the first

time in the production of a bilayer tablet that released two CVD drugs. This work has demonstrated that such an approach is possible, but it is fundamental to control the surface area-to-volume ratio to control drug release from the 3D printed layer. While our work has focused on the production of bilayer tablets, the mass-customization approach could also be utilized for single drug tablets in which the bulk of a tablet can be produced via high-volume IM processing and the tablet personalized via the addition of a 3D printed component or layer which provides the personalized dose. Thus, developing strategies for the mass-customization of drug dosage forms presents an exciting opportunity. Exploring, exploiting and cataloging the intrinsic parameters of this manufacturing method could contribute to reducing the gap separating current pharmaceutical technologies from achieving the goal of personalized medicine.

Acknowledgements

The work was supported by an AIT President's Seed Fund grant.

Transparency declarations

The authors declare no conflicts of interest.

References

Aho, J., Bøtker, J. P., Genina, N., Edinger, M., Arnfast, L., Rantanen, J., 2019. Roadmap to 3D-Printed Oral Pharmaceutical Dosage Forms: Feedstock Filament Properties and Characterization for Fused Deposition Modeling. J. Pharm. Sci. 108, 26-35. https://doi.org/10.1016/j.xphs.2018.11.012

Alford, D., Sackett, P., Nelder, G., 2000. Mass customisation—an automotive perspective. Int. J. Prod. Econ. 65, 99-110. https://doi.org/10.1016/S0925-5273(99)00093-6

Alfreda Campo, E., 2006. The Complete Part Design Handbook: for Injection Molding of Thermoplastics.

Alhnan, M.A., Okwuosa, T.C., Sadia, M., Wan, K.W., Ahmed, W., Arafat, B., 2016. Emergence of 3D Printed Dosage Forms: Opportunities and Challenges. Pharm. Res. 33, 1817–1832. https://doi.org/10.1007/s11095-016-1933-1

Alshahrani, S.M., Lu, W., Park, J.-B., Morott, J.T., Alsulays, B.B., Majumdar, S., Langley, N., Kolter, K., Gryczke, A., Repka, M. a, 2015. Stability-enhanced Hot-melt Extruded Amorphous Solid Dispersions via Combinations of Soluplus® and HPMCAS-HF. AAPS PharmSciTech 16, 824–834. https://doi.org/10.1208/s12249-014-0269-6

Aquino, R.P., Barile, S., Grasso, A., Saviano, M., 2018. Envisioning smart and sustainable healthcare: 3D Printing technologies for personalized medication. Futures. https://doi.org/10.1016/j.futures.2018.03.002

Araújo, M., Sa-Barreto, L., Gratieri, T., Gelfuso, G., Cunha-Filho, M., 2019. The Digital Pharmacies Era: How 3D Printing Technology Using Fused Deposition Modeling Can Become a Reality. Pharmaceutics 11, 128. https://doi.org/10.3390/pharmaceutics11030128

Bansal, M., Sharma, V., Singh, G., Harikumar, S.L., 2018. 3D Printing for the Future of Pharmaceuticals Dosages Forms 10.

Barbhaiya, R.H., Patel, R.B., Corrick- West, H.P., Joslin, R.S., Welling, P.G., 1982. Comparative bioavailability and pharmacokinetics of hydrochlorothiazide from oral tablet dosage forms, determined by plasma level and urinary excretion methods. Biopharm. Drug Dispos. 3, 329–336. https://doi.org/10.1002/bdd.2510030406

Brostow, W., Hagg Lobland, H.E., Narkis, M., 2006. Sliding wear, viscoelasticity, and brittleness of polymers. J. Mater. Res. 21, 2422–2428. https://doi.org/10.1557/jmr.2006.0300

Busignies, V., Mazel, V., Diarra, H., Tchoreloff, P., 2014. Development of a new test for the easy characterization of the adhesion at the interface of bilayer tablets: Proof-of-concept study by experimental design. Int. J. Pharm. 477, 476–484. https://doi.org/10.1016/j.ijpharm.2014.10.051

Busignies, V., Mazel, V., Diarra, H., Tchoreloff, P., 2013. Role of the elasticity of pharmaceutical materials on the interfacial mechanical strength of bilayer tablets. Int. J. Pharm. 457, 260–267. https://doi.org/10.1016/j.ijpharm.2013.09.009

Castrati, L., Mazel, V., Busignies, V., Diarra, H., Rossi, A., Colombo, P., Tchoreloff, P., 2016. Comparison of breaking tests for the characterization of the interfacial strength of bilayer tablets. Int. J. Pharm. 513, 709–716. https://doi.org/10.1016/j.ijpharm.2016.10.005

Chen, C.C., Tsai, T.H., Huang, Z.R., Fang, J.Y., 2010. Effects of lipophilic emulsifiers on the oral administration of lovastatin from nanostructured lipid carriers: Physicochemical characterization and pharmacokinetics. Eur. J. Pharm. Biopharm. 74, 474–482. https://doi.org/10.1016/j.ejpb.2009.12.008

Chen, C.H., Yang, J.C., Uang, Y.S., Lin, C.J., 2013. Improved dissolution rate and oral bioavailability of lovastatin in red yeast rice products. Int. J. Pharm. 444, 18–24. https://doi.org/10.1016/j.ijpharm.2013.01.028

Cheng, H., Manas-Zloczower, I., 1997. Study of mixing efficiency in kneading discs of co-rotating twin-screw extruders. Polym. Eng. Sci. 37, 1082–1090. https://doi.org/10.1002/pen.11753

Corveleyn, S., Remon, J.P., 1998. Bioavailability of hydrochlorothiazide: Conventional versus freeze-dried tablets. Int. J. Pharm. 173, 149–155. https://doi.org/10.1016/S0378-5173(98)00216-6

Crowley, M.M., Schroeder, B., Fredersdorf, A., Obara, S., Talarico, M., Kucera, S., McGinity, J.W., 2004. Physicochemical properties and mechanism of drug release from ethyl cellulose matrix tablets prepared by direct compression and hot-melt extrusion.

Int. J. Pharm. 269, 509–522. https://doi.org/10.1016/J.IJPHARM.2003.09.037

Curran, M.P., Goa, K.L., 2003. Lovastatin Extended Release. Drugs 63, 685–699. https://doi.org/10.2165/00003495-200363070-00007

Da Silveira, G., Borenstein, D., Fogliatto, F.S., 2001. Mass customization: Literature review and research directions. Int. J. Prod. Econ. 72, 1–13. https://doi.org/10.1016/S0925-5273(00)00079-7

Deradjat, D., Minshall, T., 2017. Implementation of rapid manufacturing for mass customisation. J. Manuf. Technol. Manag. 28, 95-121. https://doi.org/10.1108/JMTM-01-2016-0007

Fornes, T.D., Yoon, P.J., Paul, D.R., 2003. Polymer matrix degradation and color formation in melt processed nylon 6/clay nanocomposites. Polymer (Guildf). 44, 7545–7556. https://doi.org/10.1016/j.polymer.2003.09.034

Frankland, J., 2011. Solving Feed-Related Surging. Plast. Technol. 57, 17.

Fuenmayor, E., Forde, M., Healy, A., Devine, D., Lyons, J., McConville, C., Major, I., 2018. Material Considerations for Fused-Filament Fabrication of Solid Dosage Forms. Pharmaceutics 10, 44. https://doi.org/10.3390/pharmaceutics10020044

Fuenmayor, E., Forde, M., Healy, A. V., Devine, D.M., Lyons, J.G., McConville, C., Major, I., 2019. Comparison of fused-filament fabrication to direct compression and injection molding in the manufacture of oral tablets. Int. J. Pharm. 558, 328–340.

https://doi.org/10.1016/j.ijpharm.2019.01.013

González-González, V.A., Neira-Velázquez, G., Angulo-Sánchez, J.L., 1998. Polypropylene chain scissions and molecular weight changes in multiple extrusion *. Polym. Degrad. Stab. 60, 33–42. https://doi.org/10.1016/S0141-3910(96)00233-9

Goyanes, A., Buanz, A.B.M., Basit, A.W., Gaisford, S., 2014a. Fused-filament 3D printing (3DP) for fabrication of tablets. Int. J. Pharm. 476, 88–92. https://doi.org/10.1016/j.ijpharm.2014.09.044

Goyanes, A., Buanz, A.B.M., Basit, A.W., Gaisford, S., 2014b. Fused-filament 3D printing (3DP) for fabrication of tablets. Int. J. Pharm. 476, 88–92. https://doi.org/10.1016/j.ijpharm.2014.09.044

Goyanes, A., Robles Martinez, P., Buanz, A., Basit, A.W., Gaisford, S., 2015a. Effect of geometry on drug release from 3D printed tablets. Int. J. Pharm. 494, 657–663. https://doi.org/10.1016/j.ijpharm.2015.04.069

Goyanes, A., Robles Martinez, P., Buanz, A., Basit, A.W., Gaisford, S., 2015b. Effect of geometry on drug release from 3D printed tablets. Int. J. Pharm. https://doi.org/10.1016/j.ijpharm.2015.04.069

Goyanes, A., Robles, P., Buanz, A., Basit, A.W., Gaisford, S., 2015c. Effect of geometry on drug release from 3D printed tablets. Int. J. Pharm. 494, 657–663. https://doi.org/10.1016/j.ijpharm.2015.04.069

Goyanes, A., Wang, J., Buanz, A., Mart??nez-Pacheco, R., Telford, R., Gaisford, S., Basit, A.W., 2015d. 3D Printing of Medicines: Engineering Novel Oral Devices with Unique Design and Drug Release Characteristics. Mol. Pharm. 12, 4077–4084. https://doi.org/10.1021/acs.molpharmaceut.5b00510

Hamburg, M.A., Collins, F.S., 2010. The Path to Personalized Medicine. Perspective 363, 1–3. https://doi.org/10.1056/NEJMp1002530

Healy, A. V, Waldron, C., Geever, L.M., Devine, D.M., 2018. Degradable Nanocomposites for Fused Filament Fabrication Applications. https://doi.org/10.3390/jmmp2020029

Herman, L.L., Bashir, K., 2019. Hydrochlorothiazide. StatPearls [Internet].

Huang, Y., Dai, W.-G., 2014. Fundamental aspects of solid dispersion technology for poorly soluble drugs. Acta Pharm. Sin. B 4, 18–25. https://doi.org/10.1016/j.apsb.2013.11.001

Huang, Z., Xu, Y., Li, Y., Wang, Y., 2010. Conversion investigation for lovastatin and its derivatives by HPLC. J. Chromatogr. Sci. 48, 631–636. https://doi.org/10.1093/chromsci/48.8.631

Jonathan, G., Karim, A., 2016. 3D printing in pharmaceutics: A new tool for designing customized drug delivery systems. Int. J. Pharm. https://doi.org/10.1016/j.ijpharm.2015.12.071

Joo, Y., Shin, I., Ham, G., Abuzar, S. M., Hyun, S. M., Hwang, S. J., 2019. The advent of a novel manufacturing technology in pharmaceutics: superiority of fused deposition

modeling 3D printer. J. Pharm. Investig. 1-15. https://doi.org/10.1007/s40005-019-00451-1

Kanger, C., Hadidi, H., Akula, S., Sandman, C., Quint, J., Alsunni, M., Underwood, R., Slafter, C., Sonderup, J., Spilinek, M., Casias, J., Rao, P., Sealy, M.P., 2017. Effect of Process Parameters and Shot Peening on Mechanical Behavior of ABS Parts Manufactured by Fused Filament Fabrication (FFF), in: Proceedings of the 28th Annual International Solid Freeform Fabrication Symposium. pp. 444–458.

Khaled, S.A., Burley, J.C., Alexander, M.R., Yang, J., Roberts, C.J., 2015. 3D printing of five-in-one dose combination polypill with defined immediate and sustained release profiles. J. Control. Release 217, 308–314. https://doi.org/10.1016/j.jconrel.2015.09.028

Klose, D., Siepmann, F., Elkharraz, K., Siepmann, J., 2008. PLGA-based drug delivery systems: Importance of the type of drug and device geometry. Int. J. Pharm. 354, 95–103. https://doi.org/10.1016/j.ijpharm.2007.10.030

Konta, A., García-Piña, M., Serrano, D., 2017. Personalised 3D Printed Medicines: Which Techniques and Polymers Are More Successful? Bioengineering 4, 79. https://doi.org/10.3390/bioengineering4040079

Lim, S.H., Chia, S.M.Y., Kang, L., Yap, K.Y.L., 2016. Three-Dimensional Printing of Carbamazepine Sustained-Release Scaffold. J. Pharm. Sci. 105, 2155–2163. https://doi.org/10.1016/j.xphs.2016.04.031

Loreti, G., Maroni, A., Del Curto, M.D., Melocchi, A., Gazzaniga, A., Zema, L., 2014. Evaluation of hot-melt extrusion technique in the preparation of HPC matrices for prolonged release. Eur. J. Pharm. Sci. 52, 77–85. https://doi.org/10.1016/j.ejps.2013.10.014

Major, I., Fuenmayor, E., Mcconville, C., 2016. The Production of Solid Dosage Forms from Non-Degradable Polymers. urrent Pharm. Des. 22, 2738–2760.

Maniruzzaman, M., Boateng, J.S., Snowden, M.J., Douroumis, D., 2012. A review of hot-melt extrusion: process technology to pharmaceutical products. ISRN Pharm. 2012, 436763–436769. https://doi.org/10.5402/2012/436763

Martinez, P.R., Goyanes, A., Basit, A.W., Gaisford, S., 2018. Influence of Geometry on the Drug Release Profiles of Stereolithographic (SLA) 3D-Printed Tablets. AAPS PharmSciTech 19, 3355–3361. https://doi.org/10.1208/s12249-018-1075-3

Melchels, F.P.W., Domingos, M. a N., Klein, T.J., Malda, J., Bartolo, P.J., Hutmacher, D.W., 2012. Additive manufacturing of tissues and organs. Prog. Polym. Sci. 37, 1079–1104. https://doi.org/10.1016/j.progpolymsci.2011.11.007

Melocchi, A., Loreti, G., Del Curto, M.D., Maroni, A., Gazzaniga, A., Zema, L., 2015. Evaluation of hot-melt extrusion and injection molding for continuous manufacturing of immediate-release tablets. J. Pharm. Sci. 104, 1971–1980. https://doi.org/10.1002/jps.24419

Menard, K.P., 1999. Dynamic Mechanical Analysis. Taylor & Francis.

Menard, K.P., Menard, N.R., 2015. Dynamic Mechanical Analysis in the Analysis of Polymers and Rubbers, Encyclopedia of Polymer Science and Technology. https://doi.org/10.1002/0471440264.pst102.pub2

Mitra, A.K., Lee, C.H., Cheng, K., 2013. Advance Drug Delivery, Journal of Chemical Information and Modeling. https://doi.org/10.1017/CBO9781107415324.004

Naderi, S.H., Bestwick, J.P., Wald, D.S., 2012. Adherence to drugs that prevent cardiovascular disease: Meta-analysis on 376,162 patients. Am. J. Med. 125, 882-887.e1. https://doi.org/10.1016/j.amjmed.2011.12.013

Nakayama, Y., Takemitsu, H., Kajiwara, T., Kimura, K., Takeuchi, T., Tomiyama, H., 2018. Improving mixing characteristics with a pitched tip in kneading elements in twin-screw extrusion. AIChE J. 64, 1424–1434. https://doi.org/10.1002/aic.16003

Ndindayino, F., Vervaet, C., Van Den Mooter, G., Remon, J.P., 2002. Bioavailability of hydrochlorothiazide from isomalt-based moulded tablets. Int. J. Pharm. 246, 199–202. https://doi.org/10.1016/S0378-5173(02)00354-X

Norman, J., Madurawe, R.D., Moore, C.M.V., Khan, M.A., Khairuzzaman, A., 2017. A new chapter in pharmaceutical manufacturing: 3D-printed drug products. Adv. Drug Deliv. Rev. 108, 39–50. https://doi.org/10.1016/j.addr.2016.03.001

Okwuosa, T.C., Stefaniak, D., Arafat, B., Isreb, A., Wan, K.W., Alhnan, M.A., 2016. A

Lower Temperature FDM 3D Printing for the Manufacture of Patient-Specific Immediate Release Tablets. Pharm. Res. 33, 2704–2712. https://doi.org/10.1007/s11095-016-1995-0

Palo, M., Holländer, J., Suominen, J., Yliruusi, J., 2017. Expert Review of Medical Devices 3D printed drug delivery devices : perspectives and technical challenges. Expert Rev. Med. Devices 14, 685–696. https://doi.org/10.1080/17434440.2017.1363647

Patel, R.B., Patel, U.R., Rogge, M.C., Shah, V.P., Prasad, V.K., Selen, A., Welling, P.G., 1984. Bioavailability of Hydrochlorothiazide from Tablets and Suspensions. J. Pharm. Sci. 73, 359–361. https://doi.org/10.1002/jps.2600730317

Prasad, L.K., Smyth, H., 2016. 3D Printing technologies for drug delivery: a review. Drug Dev. Ind. Pharm. 42, 1019–1031. https://doi.org/10.3109/03639045.2015.1120743

Prasad, E., Islam, M. T., Goodwin, D. J., Megarry, A. J., Halbert, G. W., Florence, A. J., Robertson, J., 2019. Development of a Hot-Melt Extrusion (HME) process to produce drug loaded Affinisol™ 15LV filaments for Fused Filament Fabrication (FFF) 3D printing. Addit. Manuf. 29, 100776. https://doi.org/10.1016/j.addma.2019.06.027

Quinn, M., 2018. Fused Filament Fabrication of Polycarbonate Components in a Simulated Orbital Environment.

Quinten, T., Beer, T. De, Vervaet, C., Remon, J.P., 2009. Evaluation of injection moulding as a pharmaceutical technology to produce matrix tablets. Eur. J. Pharm. Biopharm. 71,

145–154. https://doi.org/10.1016/j.ejpb.2008.02.025

Quinten, T, De Beer, T., Almeida, A., Vlassenbroeck, J., Van Hoorebeke, L., Remon, J.P., Vervaet, C., 2011. Development and evaluation of injection-molded sustained-release tablets containing ethylcellulose and polyethylene oxide. Drug Dev. Ind. Pharm. 37, 149–159. https://doi.org/10.3109/03639045.2010.498426know

Quinten, Thomas, De Beer, T., Remon, jp, Vervaet, C., 2011. Overview of injection molding as a manufacturing technique for pharmaceutical applications. Inject. Molding Process. Des. Appl. 1–42.

Qureshi, M.J., Mallikarjun, C., Kian, W.G., 2015. Enhancement of solubility and therapeutic potential of poorly soluble lovastatin by SMEDDS formulation adsorbed on directly compressed spray dried magnesium aluminometasilicate liquid loadable tablets: A study in diet induced hyperlipidemic rabbits. Asian J. Pharm. Sci. 10, 40–56. https://doi.org/10.1016/j.ajps.2014.08.003

Radlmaier, V., Heckel, C., Winnacker, M., Erber, A., Koerber, H., 2017. Effects of thermal cycling on polyamides during processing. Thermochim. Acta 648, 44–51. https://doi.org/10.1016/j.tca.2016.12.011

Ravi, P., Shiakolas, P.S., Welch, T.R., 2017. Poly-L-lactic acid: Pellets to fiber to fused filament fabricated scaffolds, and scaffold weight loss study. Addit. Manuf. 16, 167–176. https://doi.org/10.1016/j.addma.2017.06.002

Reynolds, T.D., Mitchell, S.A., Balwinski, K.M., 2002. Investigation of the effect of tablet surface area/volume on drug release from hydroxypropylmethylcellulose controlled-release matrix tablets. Drug Dev. Ind. Pharm. 28, 457–466. https://doi.org/10.1081/DDC-120003007

Sadia, M., Arafat, B., Ahmed, W., Forbes, R.T., Alhnan, M.A., 2018a. Channelled tablets: An innovative approach to accelerating drug release from 3D printed tablets. J. Control. Release 269, 355–363. https://doi.org/10.1016/j.jconrel.2017.11.022

Sadia, M., Arafat, B., Ahmed, W., Forbes, R.T., Alhnan, M.A., 2018b. Channelled tablets: An innovative approach to accelerating drug release from 3D printed tablets. J. Control. Release 269, 355–363. https://doi.org/10.1016/j.jconrel.2017.11.022

Sarode, A.L., Sandhu, H., Shah, N., Malick, W., Zia, H., 2013. Hot melt extrusion (HME) for amorphous solid dispersions: Predictive tools for processing and impact of drug–polymer interactions on supersaturation. Eur. J. Pharm. Sci. 48, 371–384. https://doi.org/10.1016/j.ejps.2012.12.012

Saviano, M., Aquino, R.P., Del Gaudio, P., Sansone, F., Russo, P., 2019. Poly(vinyl alcohol) 3D printed tablets: The effect of polymer particle size on drug loading and process efficiency. Int. J. Pharm. 561, 1–8. https://doi.org/10.1208/s12249-018-1075-3

Siepmann, J., Peppas, N.A., 2012. Modeling of drug release from delivery systems based on hydroxypropyl methylcellulose (HPMC). Adv. Drug Deliv. Rev. 64, 163–174. https://doi.org/10.1016/j.addr.2012.09.028

Siepmann, J., Podual, K., Sriwongjanya, M., Peppas, N.A., Bodmeier, R., 1999. A New Model Describing the Swelling and Drug Release Kinetics from Hydroxypropyl Methylcellulose Tablets. J. Pharm. Sci. 88, 65–72. https://doi.org/10.1021/js9802291

Simpson, R.J., 2006. Challenges for Improving Medication Adherence. JAMA 296, 2614. https://doi.org/10.1001/jama.296.21.jed60074

Skowyra, J., Pietrzak, K., Alhnan, M. a., 2015. Fabrication of extended-release patient-tailored prednisolone tablets via fused deposition modelling (FDM) 3D printing. Eur. J. Pharm. Sci. https://doi.org/10.1016/j.ejps.2014.11.009

Sun, Y., Soh, S., 2015. Printing Tablets with Fully Customizable Release Profiles for Personalized Medicine. Adv. Mater. 27, 7847–7853. https://doi.org/10.1002/adma.201504122

Tidau, M., Kwade, A., Finke, J. H., 2019. Influence of High, Disperse API Load on Properties along the Fused-Layer Modeling Process Chain of Solid Dosage Forms. Pharmaceutics. 11, 194. https://doi.org/10.3390/pharmaceutics11040194

Ventola, C.L., 2014. Medical Applications for 3D Printing: Current and Projected Uses. P T 39, 704–11. https://doi.org/10.1016/j.infsof.2008.09.005

Villmow, T., Kretzschmar, B., Pötschke, P., 2010. Influence of screw configuration, residence time, and specific mechanical energy in twin-screw extrusion of polycaprolactone/multi-walled carbon nanotube composites. Compos. Sci. Technol. 70,

2045–2055. https://doi.org/10.1016/j.compscitech.2010.07.021

Wang, S., Capoen, L., D'hooge, D.R., Cardon, L., 2018. Can the melt flow index be used to predict the success of fused deposition modelling of commercial poly(lactic acid) filaments into 3D printed materials? Plast. Rubber Compos. 47, 9–16. https://doi.org/10.1080/14658011.2017.1397308

Yadava, S.K., Naik, J.B., Patil, J.S., Mokale, V.J., Singh, R., 2015. Enhanced solubility and bioavailability of lovastatin using stabilized form of self-emulsifying drug delivery system. Colloids Surfaces A Physicochem. Eng. Asp. 481, 63–71. https://doi.org/10.1016/j.colsurfa.2015.04.026

Young, C.R., Koleng, J.J., McGinity, J.W., 2002. Production of spherical pellets by a hot-melt extrusion and spheronization process. Int. J. Pharm. 242, 87–92. https://doi.org/10.1016/S0378-5173(02)00152-7

Yu, D.G., Zhu, L.-M., Branford-White, C.J., Yang, X.L., 2008. Three-Dimensional Printing in Pharmaceutics: Promises and Problems. J. Pharm. Sci. 97, 3666–3690. https://doi.org/10.1002/jps.21284

Zema, L., Loreti, G., Melocchi, A., Maroni, A., Gazzaniga, A., 2012. Injection Molding and its application to drug delivery. J. Control. Release 159, 324–331. https://doi.org/10.1016/j.jconrel.2012.01.001

Figure Captions

Fig. 1. CAD design of a flat-bilayer tablet. Values are expressed in mm.

Fig 2. Flow chart depicting the industrial setting for the mass-customisation of solid dosage forms combining FFF with IM using automation to incorporate the inserts into IM tool in order to accelerate the manufacturing of samples. The most important features of each stage of manufacturing are mentioned under each one of the images where they are more relevant.

Fig 3. Comparison of thermal and flow properties of drugs, placebo and drug-loaded blend used in this body of work. The analysis was performed on samples after each HME processing step. (a) shows the thermal properties after the first step; (b) after the second step; and (c) displays MFI profiles for both drug-loaded formulations and placebo.

Fig 4. DMA (dynamic mechanical analysis) thermograms for formulations after two melt-processing steps, displaying storage modulus (E', green), loss modulus (E", blue), and tan δ (maroon) across a broad temperature (◦C) sweep: (a) No drug; (b) LOVA loaded formulation; (c) HCTZ loaded formulation.

Fig 5. Pictures of bilayer tablet produced using a multi-step manufacturing procedure composed by FFF followed by IM. The FFF layer (a) is loaded with HCTZ and the injected moulded half (b) is loaded with LOVA. (c) and (d) are images of the side view of the tablet from batch 1. Second row of images represents tablets fabricated using different injection pressures :(e) 120 Bar (f) 60 Bar (d) 20 Bar. All inserts are 100% infill. Scale line represents 10 mm. (h) to (p) are SEM images of placebo bilayer tablets cross-sectional area: (h) batch 1, (i) batch 2, (j) batch 3, (k) batch 4, (l) batch 5, (m) batch 6, (n) batch, (o) batch 8, (p) batch 9. Scale bars for (a) to (g) represent 10 mm and from (h) to (p) 1 mm

Fig 6. Stress-Strain curves obtained from the interfacial layer separation test for all tablets.

Fig 7. Drug release profiles for both drugs and tablets in this study over a 72 hour period.

Fig 8. Drug release profiles for both drugs, averaged (n: 3) from curves in figure 9 based on infill percentage for HCTZ and injection pressure for LOVA over a 72 hour period.

Fig 9. Drug release for both drug s for tablets manufactured using an injection pressure of 20 bar and three increasing infill percentages along with SEM images of the cross-sectional areas for all tablets, averaged (n: 3) based on infill percentage for HCTZ and injection pressure for LOVA over a 72 hour. Scale bars represent 1 mm

Fig 10. Drug release for both drug s for tablets manufactured using an injection pressure of 60 bar and three increasing infill percentages along with SEM images of the cross-sectional areas for all tablets, averaged (n: 3) based on infill percentage for HCTZ and injection pressure for LOVA over a 72 hour period. Scale bars represent 1 mm

Fig 11. Drug release for both drugs for tablets manufactured using an injection pressure of 120 bar and three increasing infill percentages along with SEM images of the cross-sectional areas for all tablets, averaged (n: 3) based on infill percentage for HCTZ and injection pressure for LOVA over a 72 hour period. Scale bars represent 1 mm

Table 1.

Formulation profile used in the production of material for FFF and IM applications. All values represent the weight/weight percentage composing each formulation.

PVP-VA (%)	PCL (%)	PEO (%)	Lovastatin (%)	Hydrochlorothiazide (%)
30	60	10	-	-
28.5	57.0	9.5	5	-
28.5	57.0	9.5	-	5

Table 2.

The range of bilayer tablets fabricated via a combination of FFF and IM.

Batch name	Infill Percentage (%)	Injection pressure (bar)
Batch 1	25	20
Batch 2	25	60
Batch 3	25	120
Batch 4	50	20
Batch 5	50	60
Batch 6	50	120
Batch 7	100	20
Batch 8	100	60
Batch 9	100	120

Table 3.

Brittleness (B) (%Pa) of extruded filaments at room temperature. B values are shown as multiples of 10^4 for the convenience of the reader. Storage modulus (E') was obtained at room temperature at a 1 Hz frequency (n = 3). Strain-at-break (ε_b) was obtained using a room temperature three-point bend testing (n = 5).

Formulation	**B (%Pa)(10^4)**	**ε_b(%)**	**E' (Pa)**
Formulation (no drug) after the first processing step	0.139	72.23 ± 6.67	995.94 ± 1.87
Formulation (no drug) after the second processing step	0.175	68.22 ± 4.23	837.97 ± 29.92

Table 4.

Force necessary to break tablets along the interfacial contact surface between layers along with the displacement at the end of the test. Mean values presented (n: 5)

	Breaking force (N)	**Maximum Displacement (mm)**
Batch 1	99.56 ± 24.7165	4.805 ± 0.513739
Batch 2	113.8 ± 15.06529	4.026 ± 0.913138
Batch 3	67.79 ± 6.073029	3.461 ± 1.167218
Batch 4	100.5 ± 55.66739	3.296 ± 0.52017
Batch 5	114.2 ± 15.32889	3.508 ± 0.899449
Batch 6	106.7 ± 25.64383	4.350 ± 0.79012
Batch 7	100.6 ± 31.15431	3.492 ± 0.31071
Batch 8	76.21 ± 26.63361	2.944 ± 0.627423
Batch 9	77.75 ± 16.61252	3.640 ± 0.65109

***Graphical Abstract (for review)**

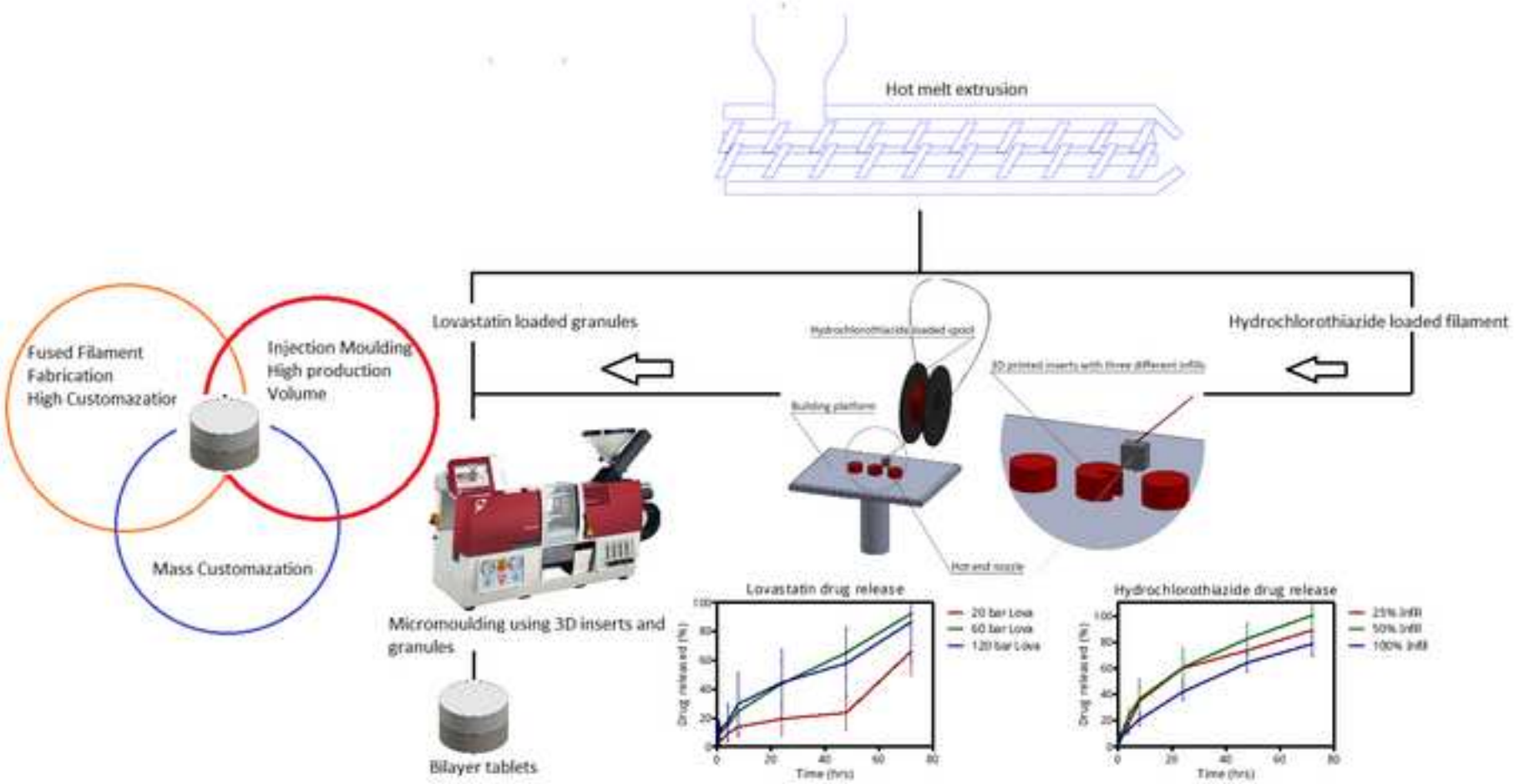

Figure 1

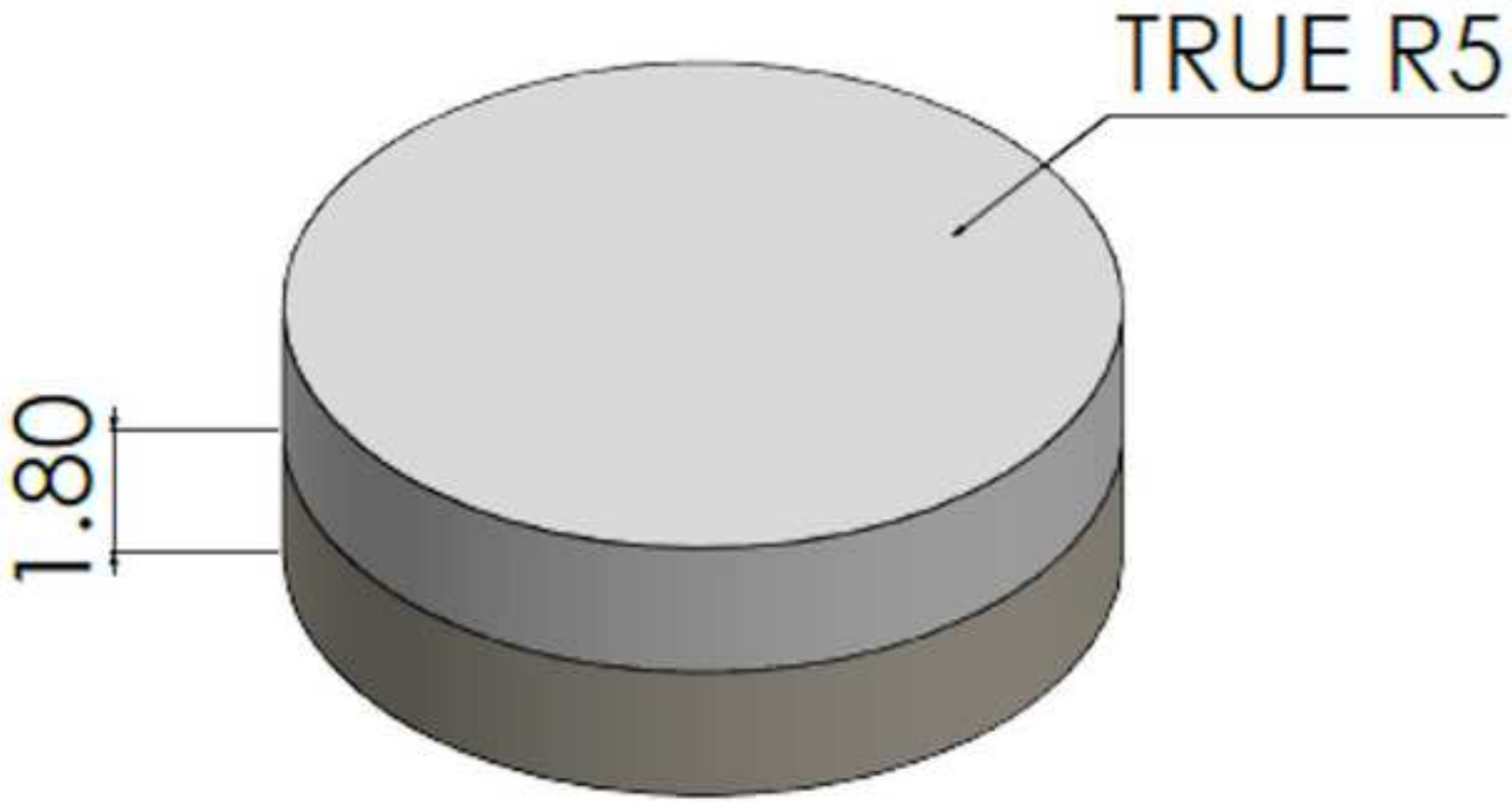

Figure 2

3D printing	Robotics	Injection Moulding
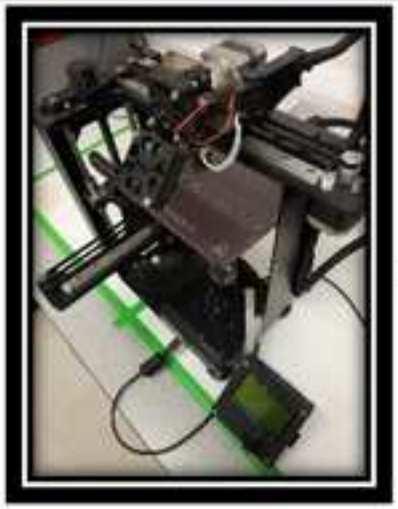		
• Discontinuous process. • Offline production of samples. • Low production volume. • Slow process • Highly customisable parts with same volume but different properties. • Multiple printing units could accelerate production volume.	• Allows for automation of the process. • Pick and place relevant inserts in IM tool with no operator intervention as needed. • Accelerates the bridging between 3D printing and injection moulding. • Improves continuity of tablet fabrication via FFF combined with IM.	• Continuous process. • High production volume. • High part dimensional accuracy. • Tooling with several cavities produces several tablets in minutes, hundreds in an hour.

Figure 3a

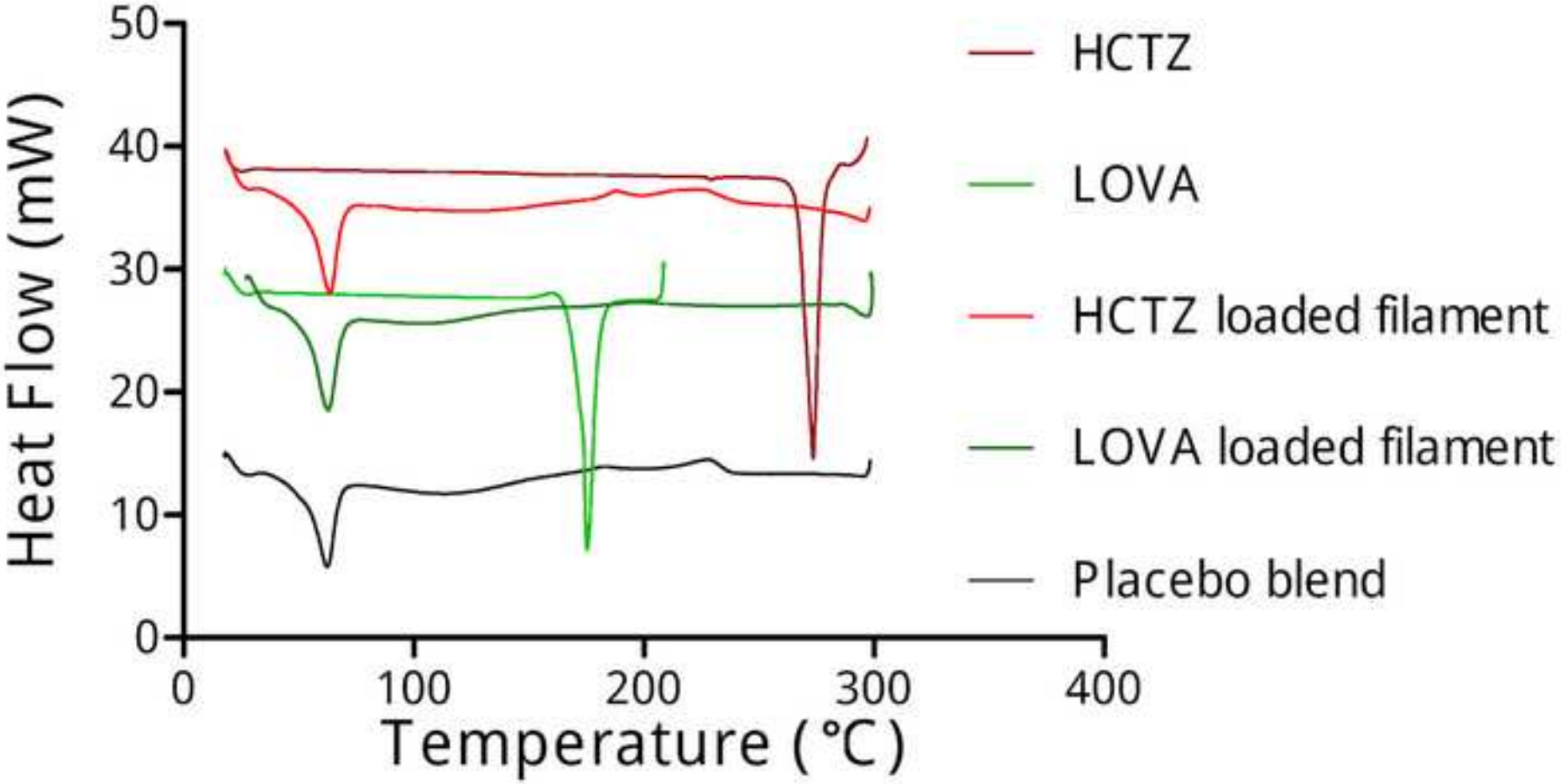
Heat Flow (mW)
50
40
30
20
10
0
0
100
200
300
400
Temperature (°C)
HCTZ
LOVA
HCTZ loaded filament
LOVA loaded filament
Placebo blend

Figure 3b

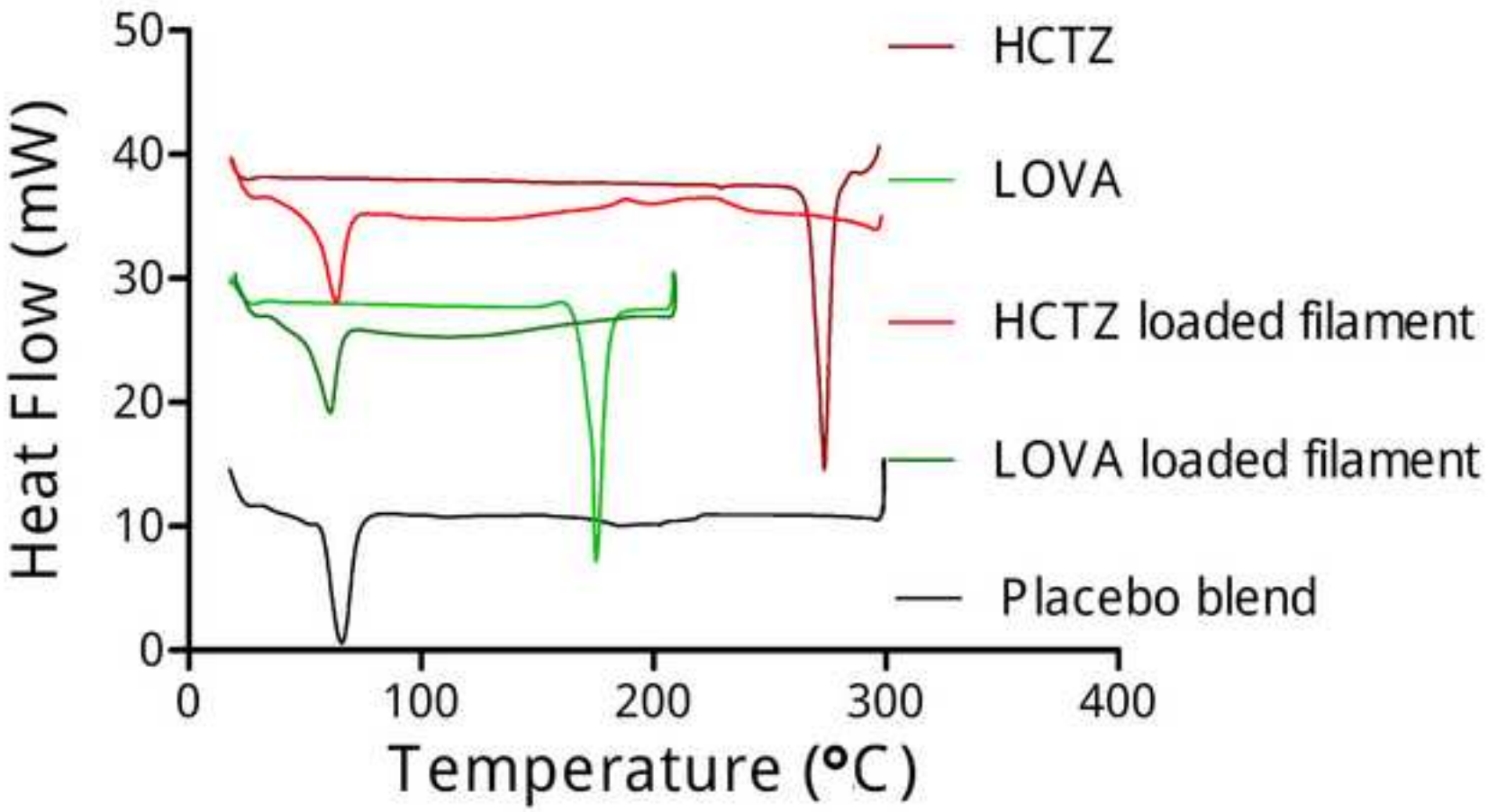
Heat Flow (mW)
50
40
30
20
10
0
0
100
200
300
400
Temperature (°C)
HCTZ
LOVA
HCTZ loaded filament
LOVA loaded filament
Placebo blend

Figure 3c

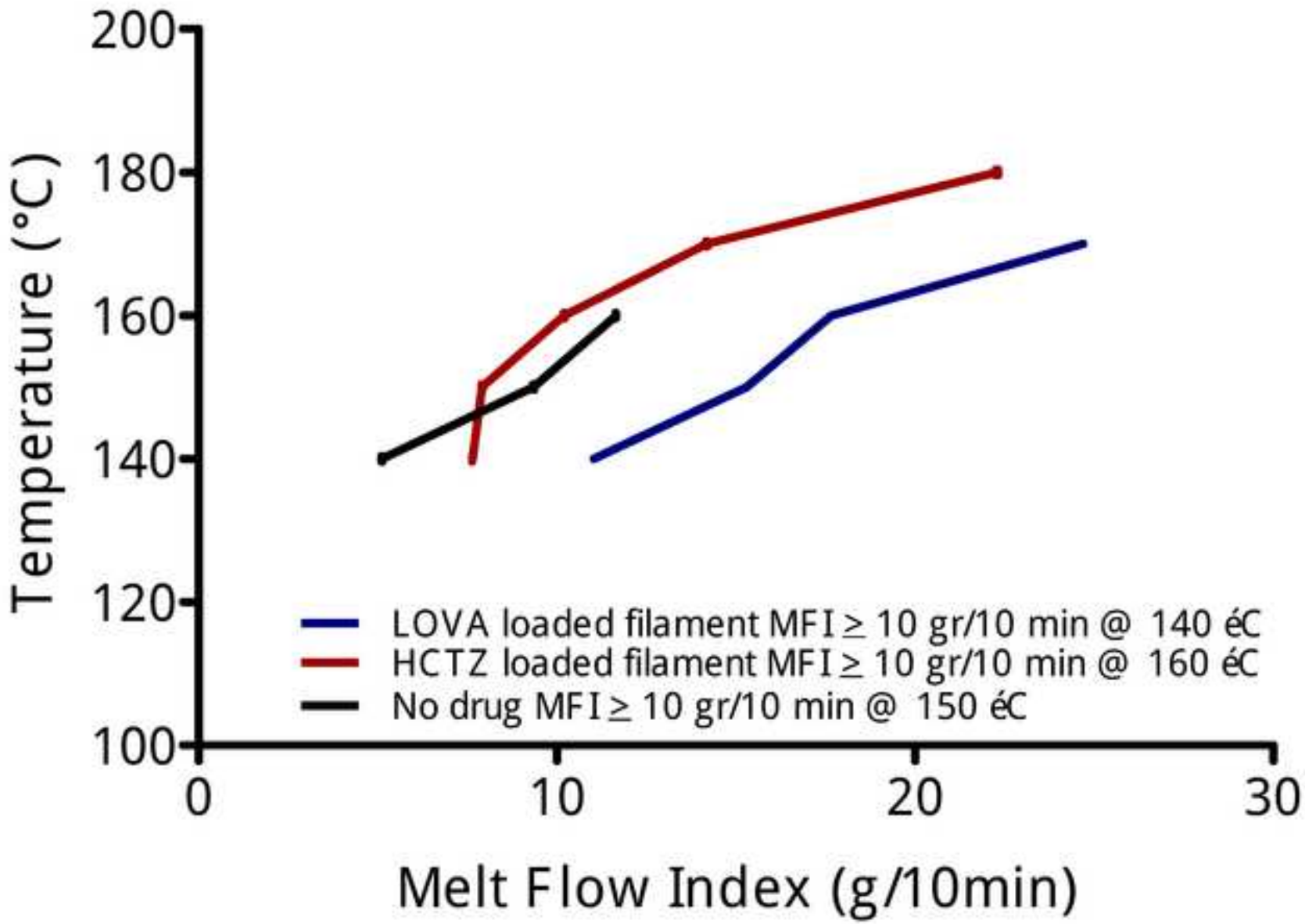

Figure 4a

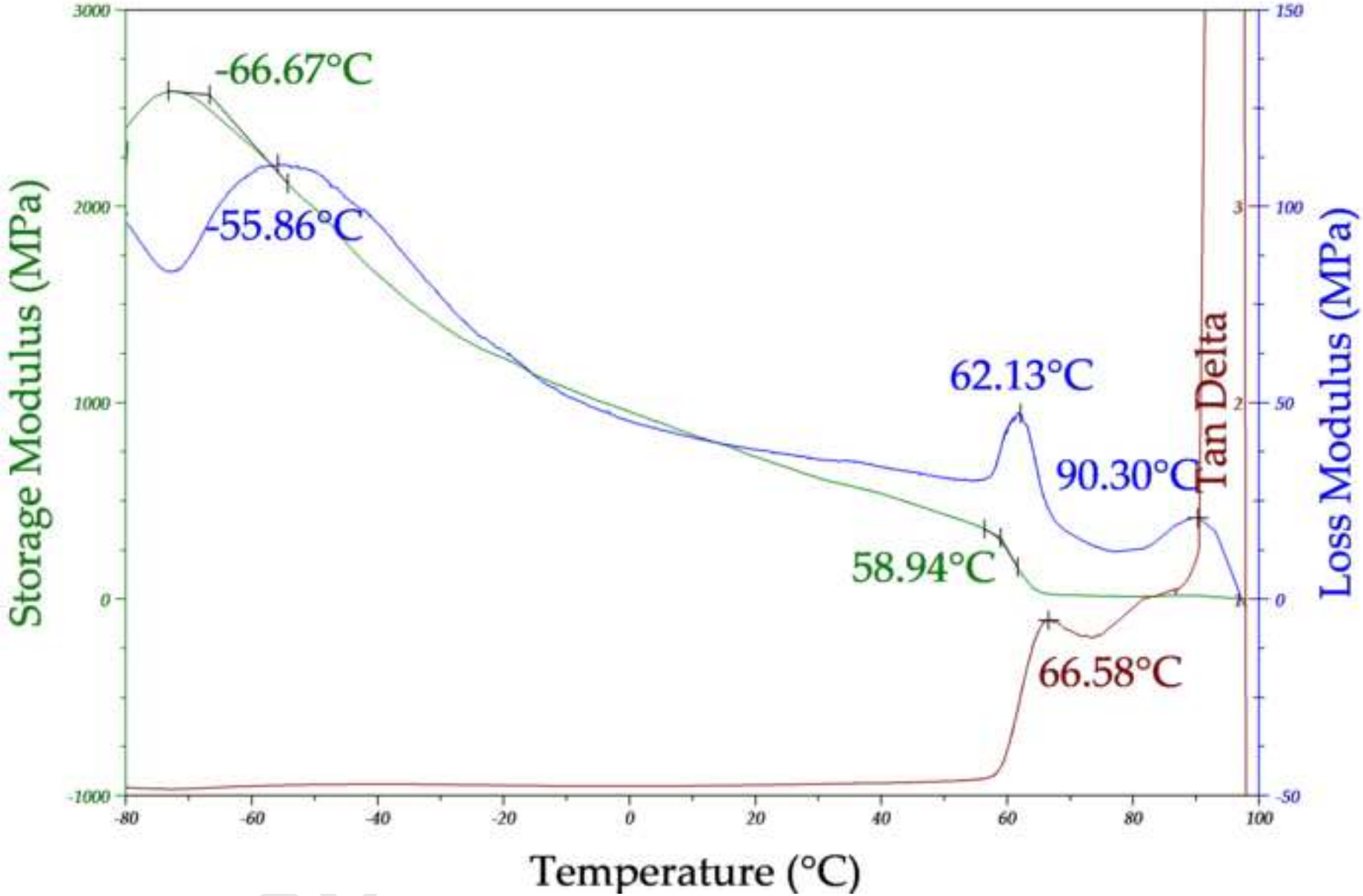

Figure 4b

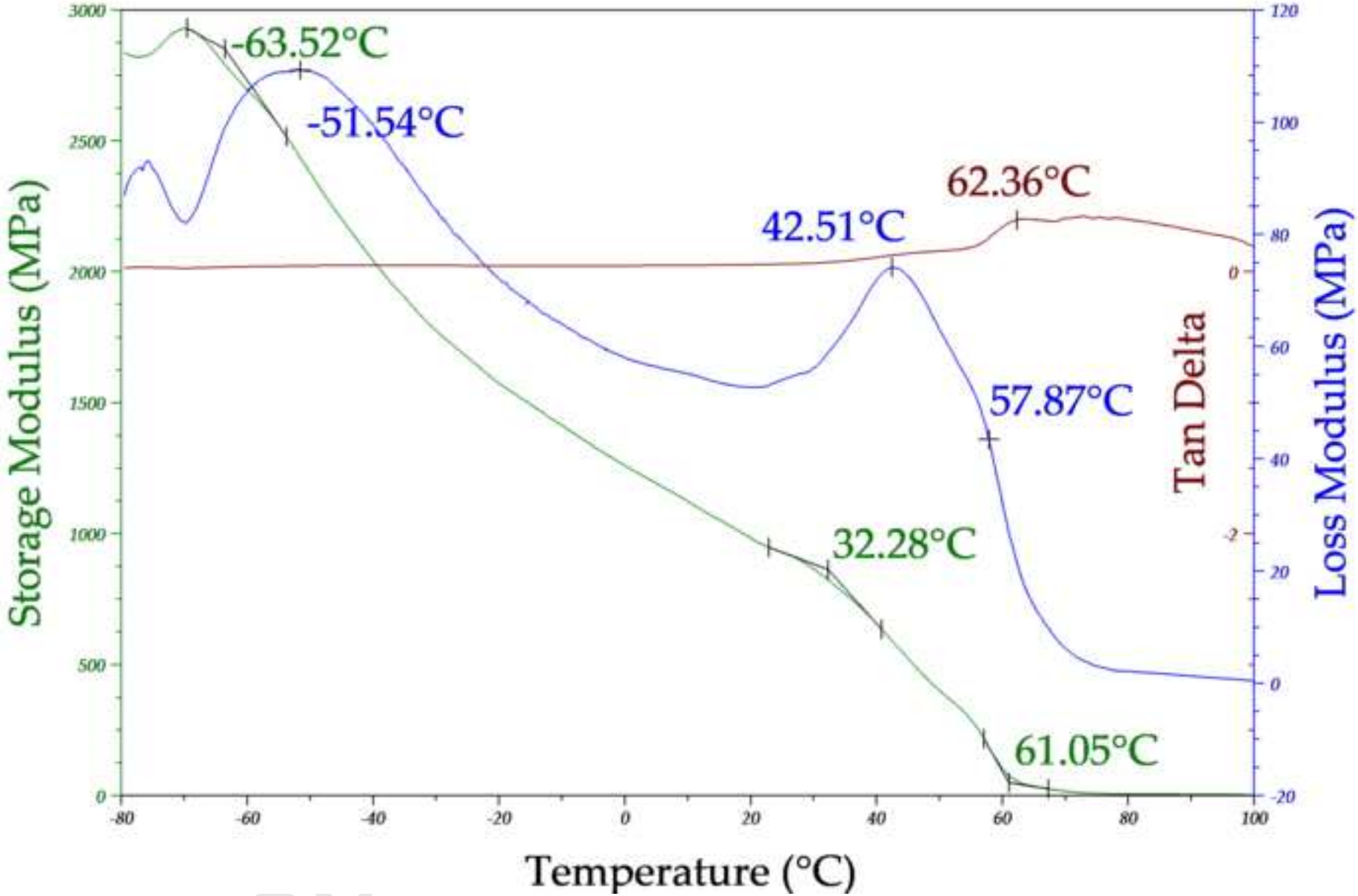

Figure 4c

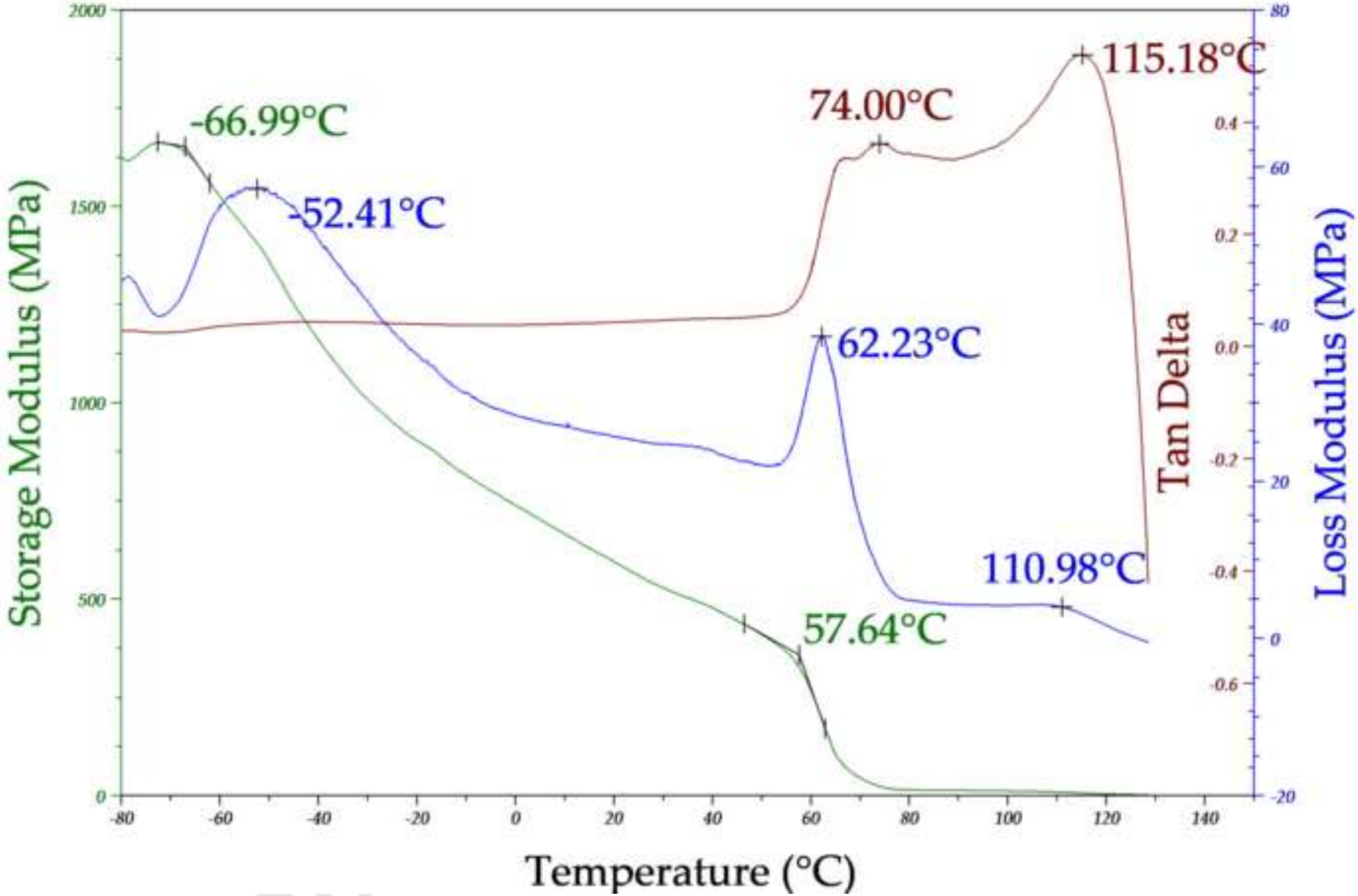

Figure 5

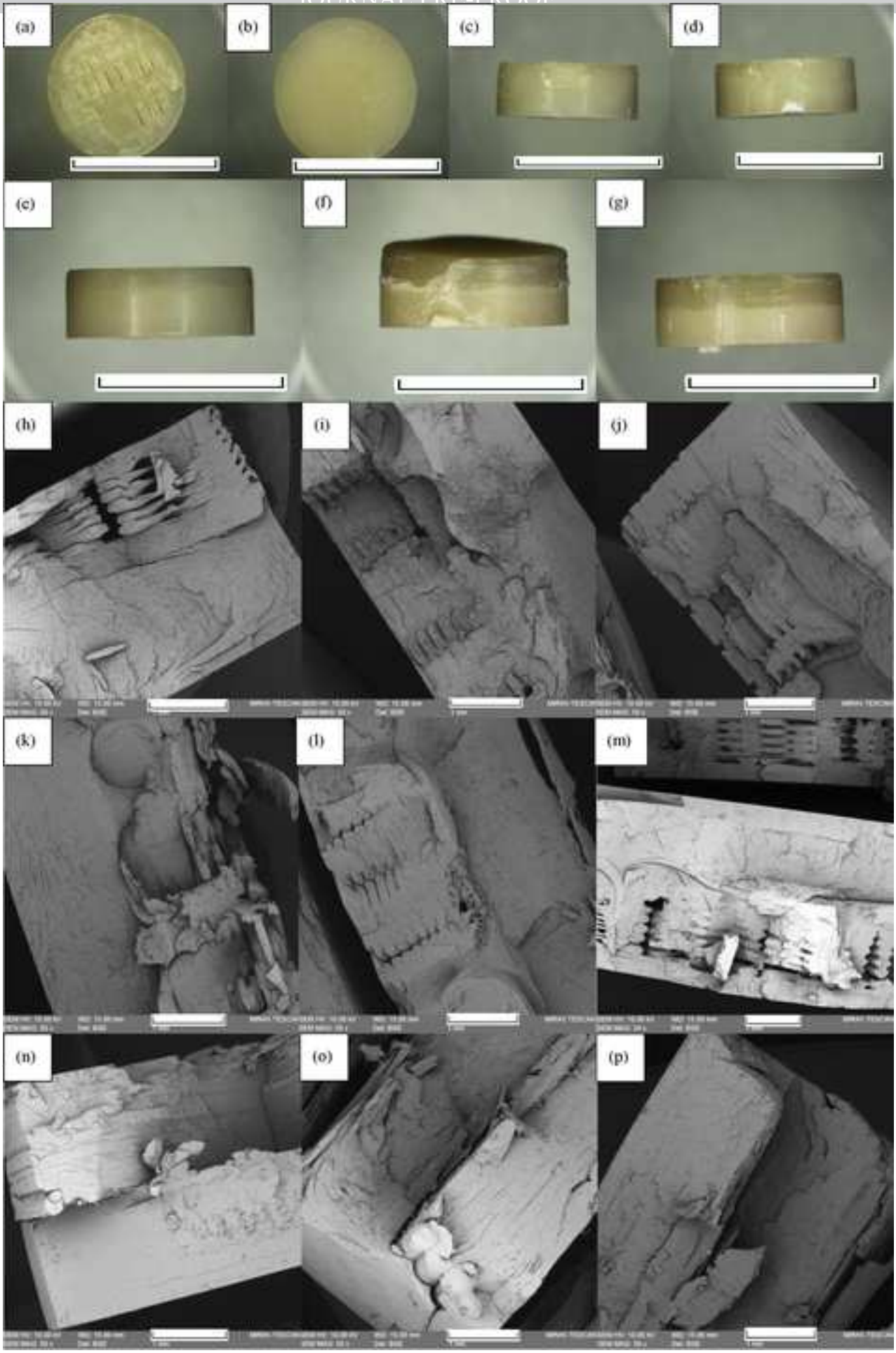

Figure 6

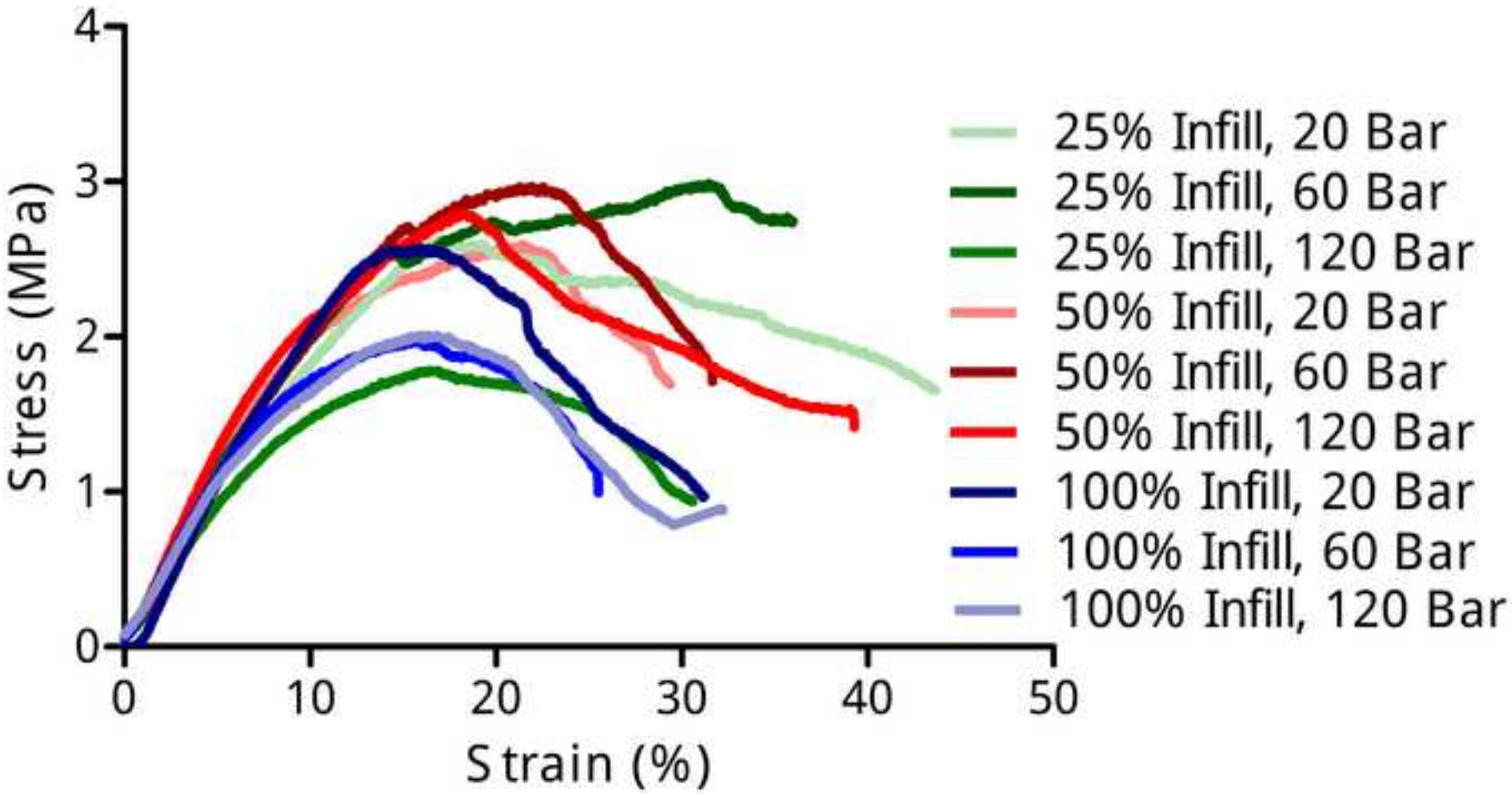
Stress (MPa)
0
1
2
3
4
0
10
20
30
40
50
Strain (%)
25% Infill, 20 Bar
25% Infill, 60 Bar
25% Infill, 120 Bar
50% Infill, 20 Bar
50% Infill, 60 Bar
50% Infill, 120 Bar
100% Infill, 20 Bar
100% Infill, 60 Bar
100% Infill, 120 Bar

Figure 7 hctz

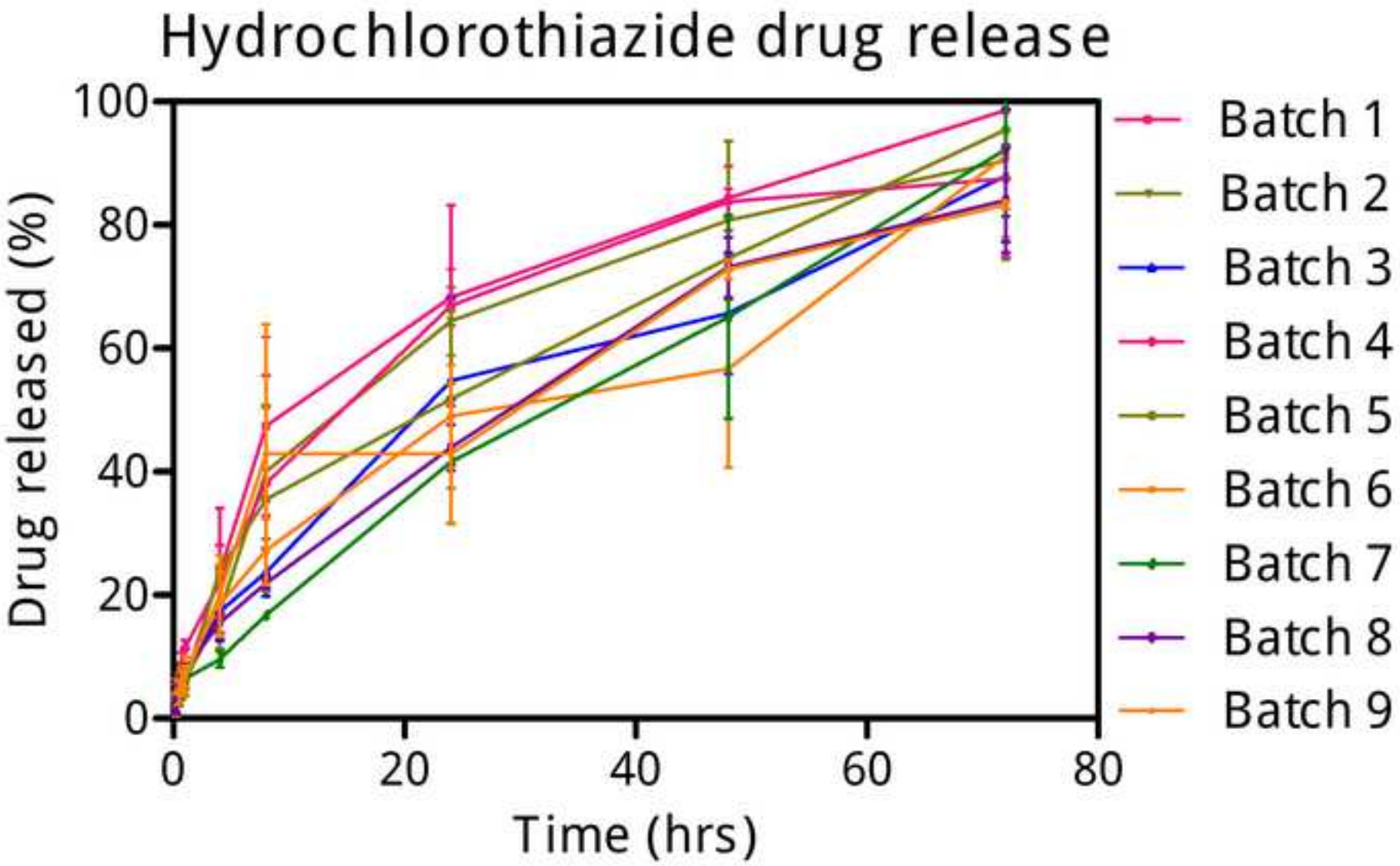

Figure 7 lova

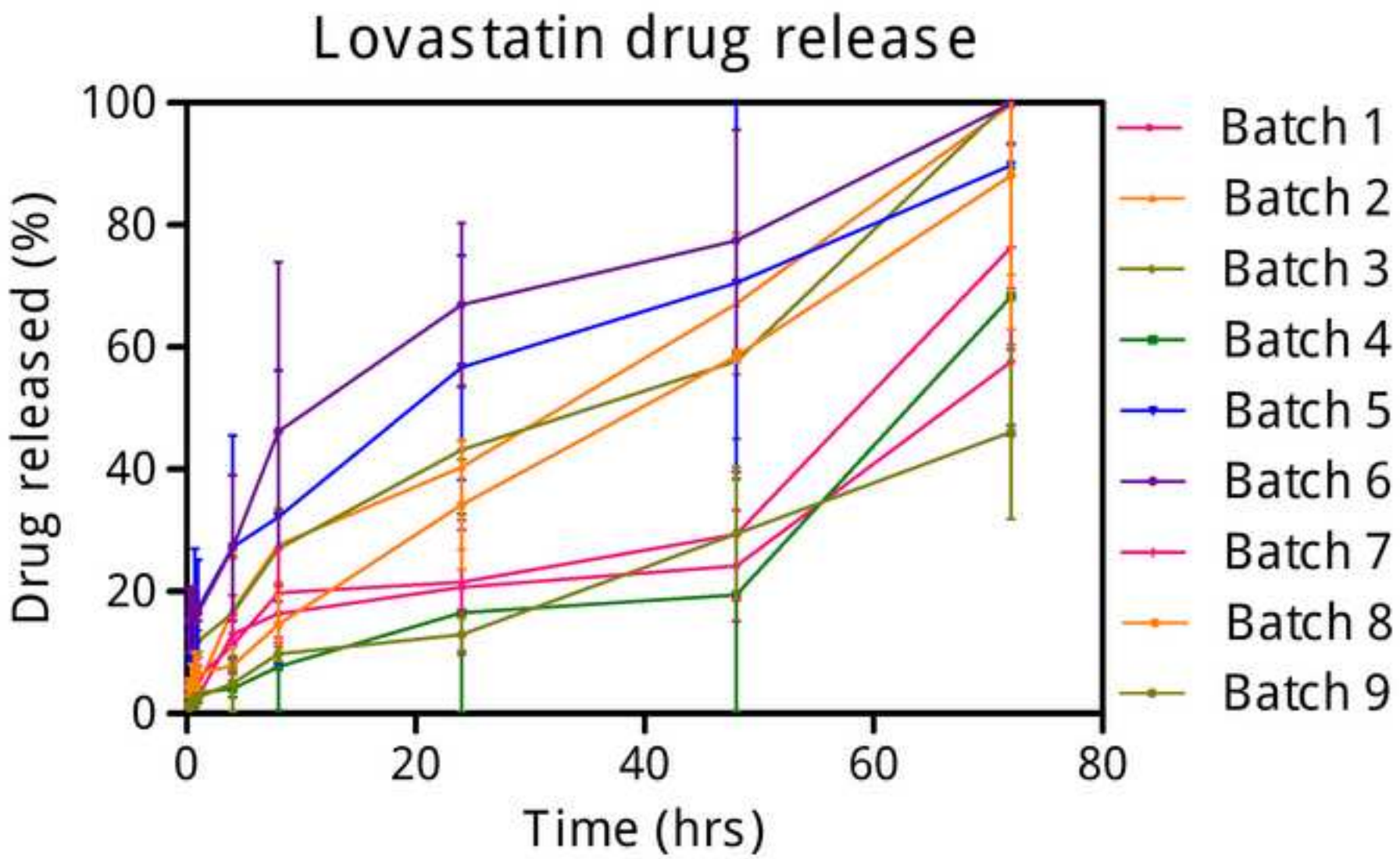

Figure 8 hctz

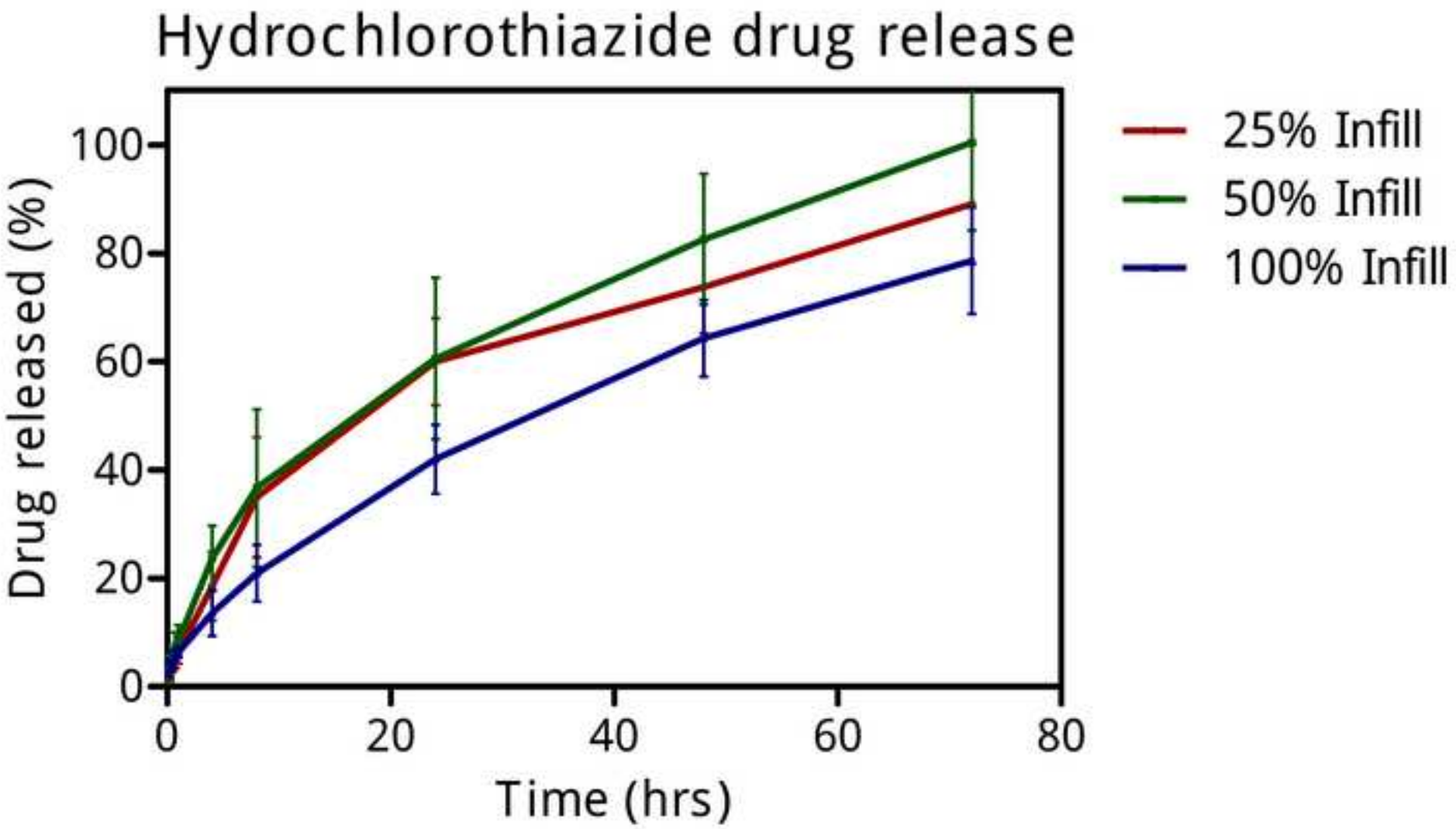

Figure 8 lova

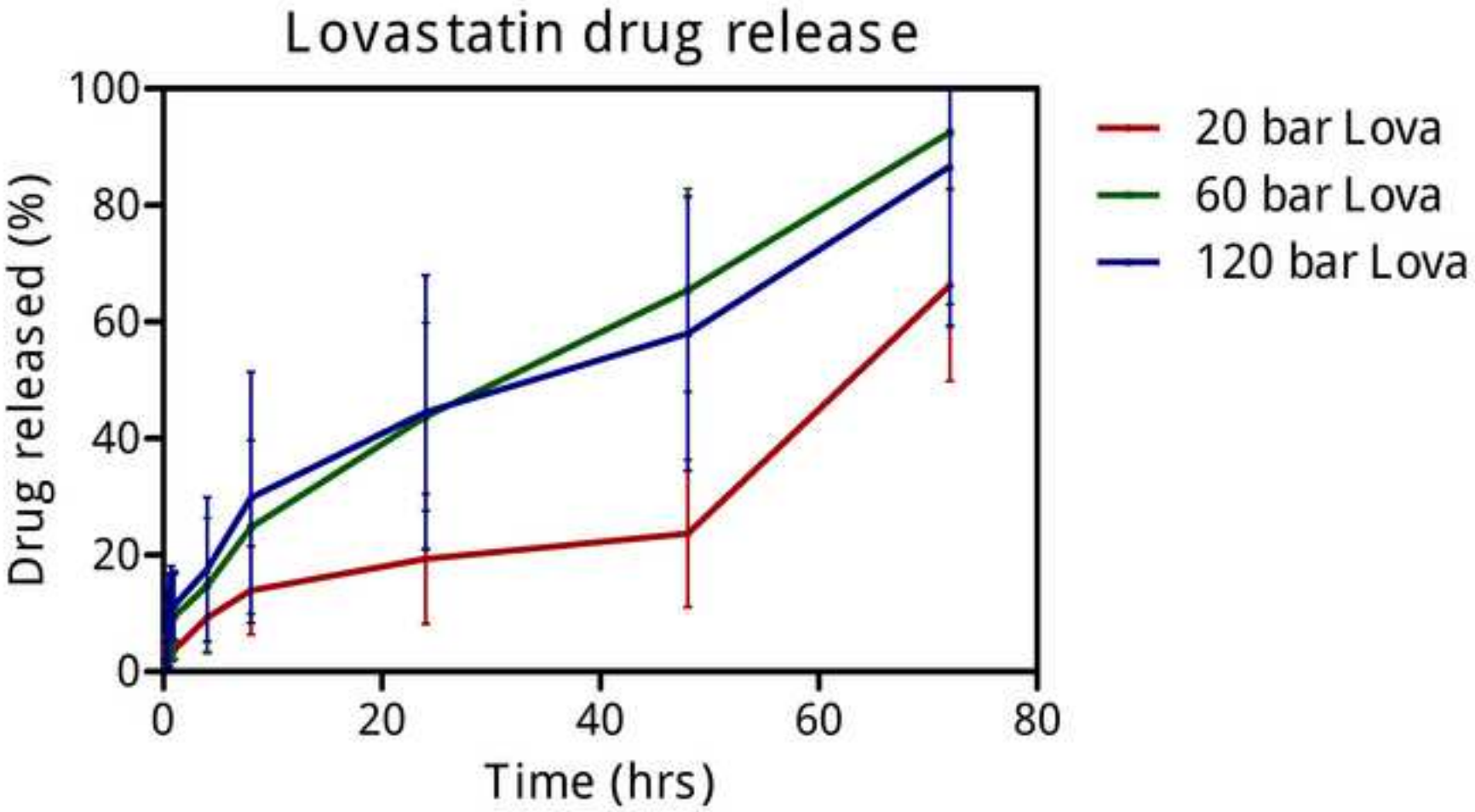

Figure 9 top

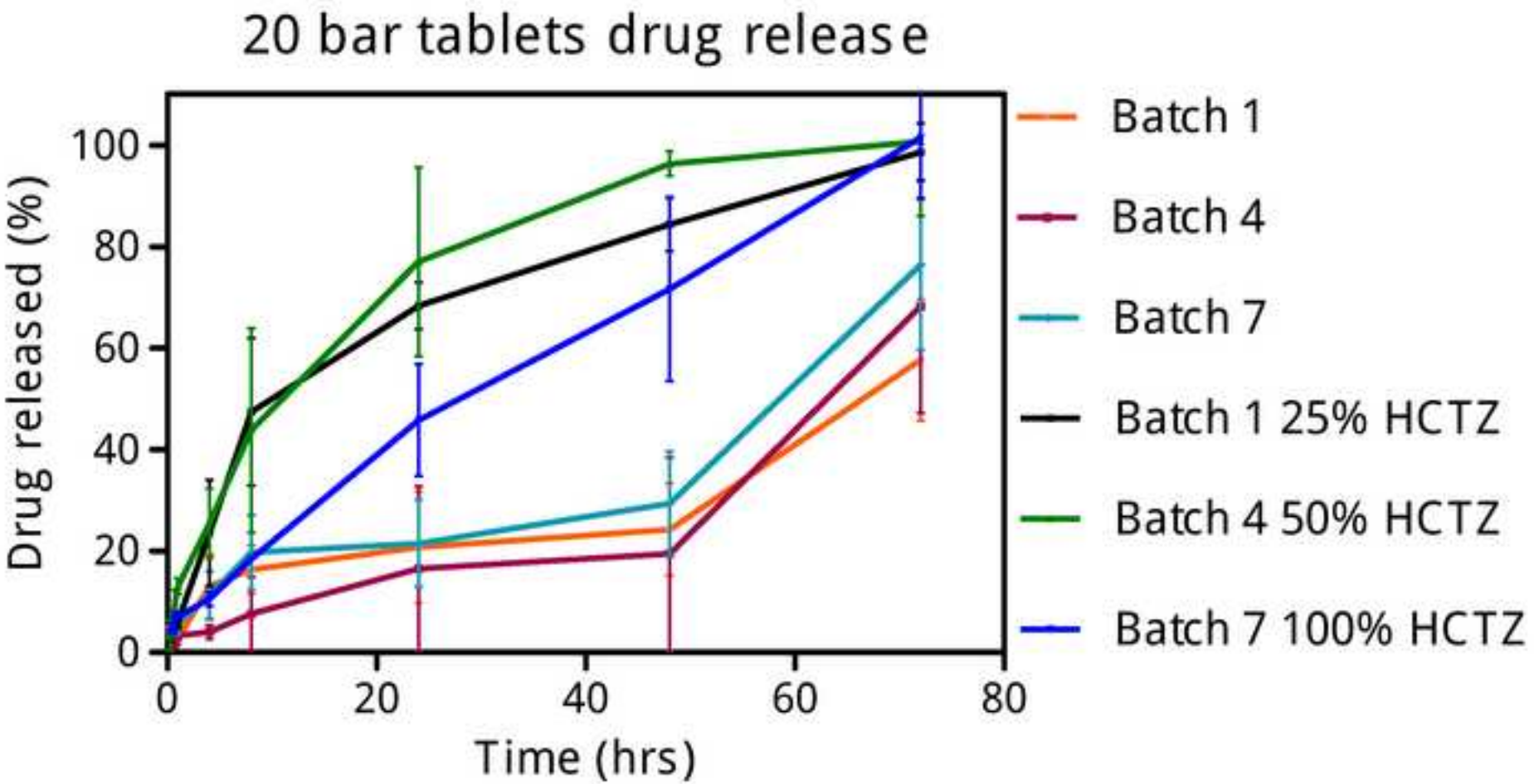
20 bar tablets drug release
Drug released (%)
0
20
40
60
80
100
0
20
40
60
80
Time (hrs)
Batch 1
Batch 4
Batch 7
Batch 1 25% HCTZ
Batch 4 50% HCTZ
Batch 7 100% HCTZ

Figure 9 bottom

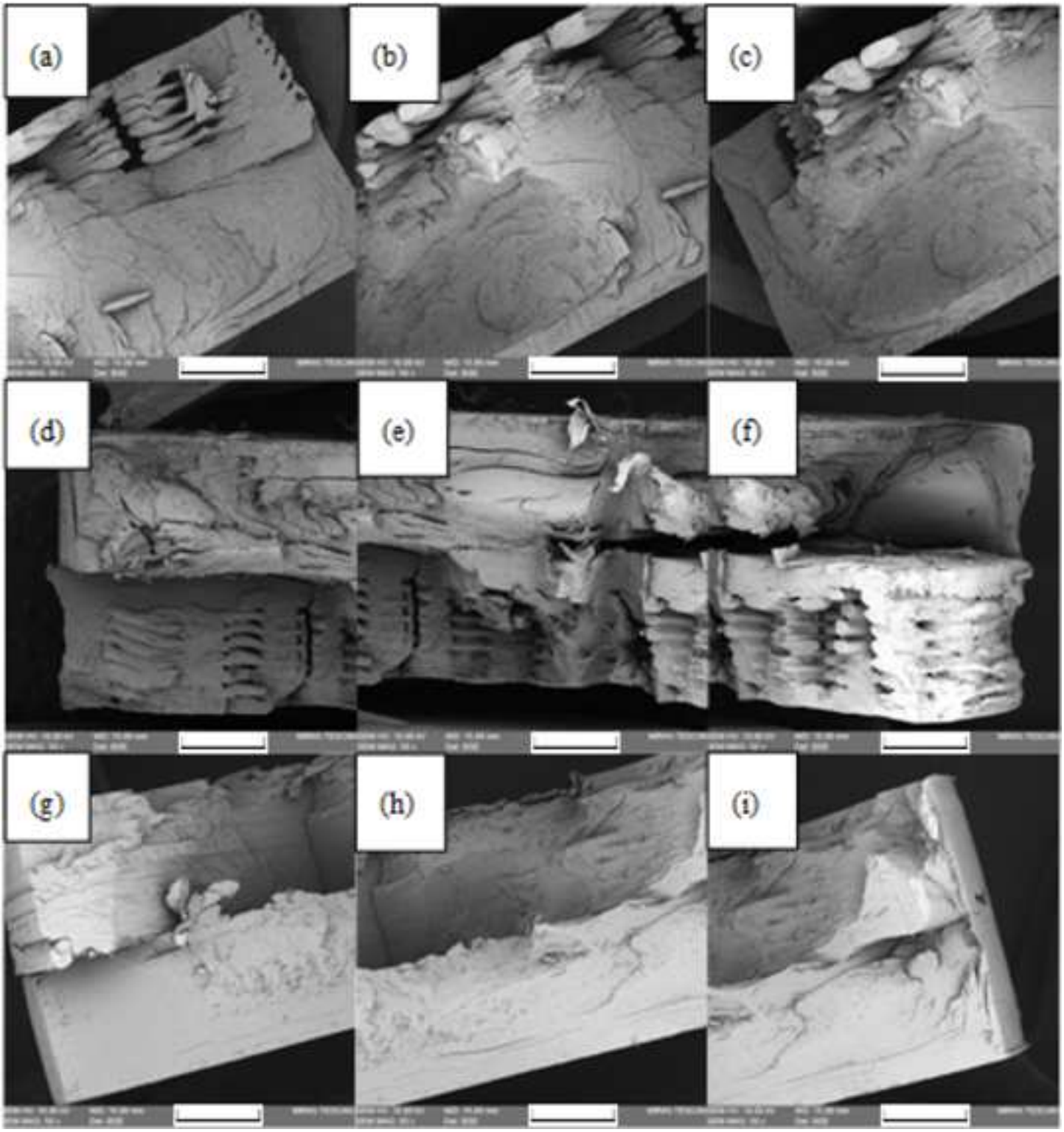

Figure 10 top

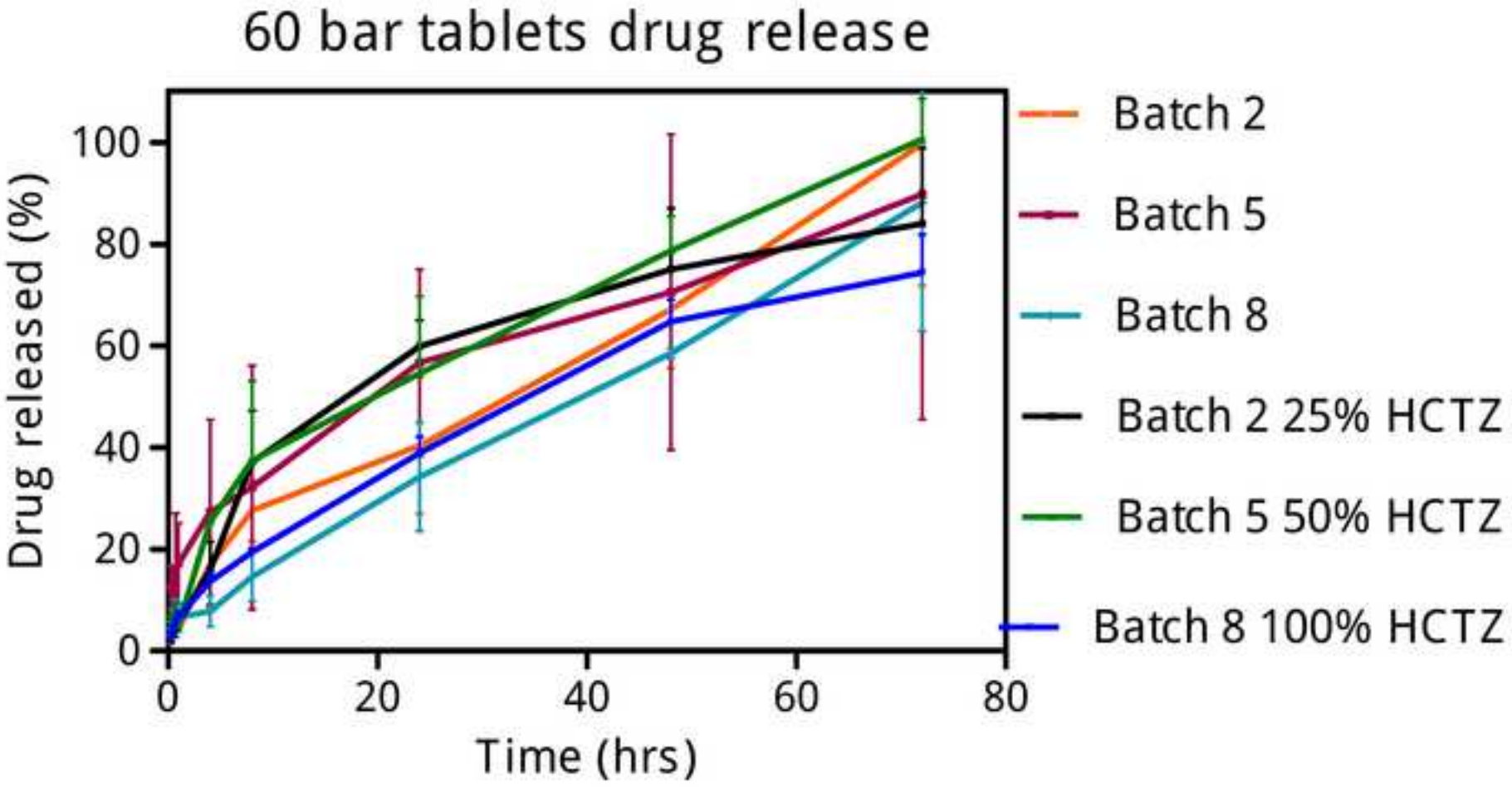

Figure 10 bottom

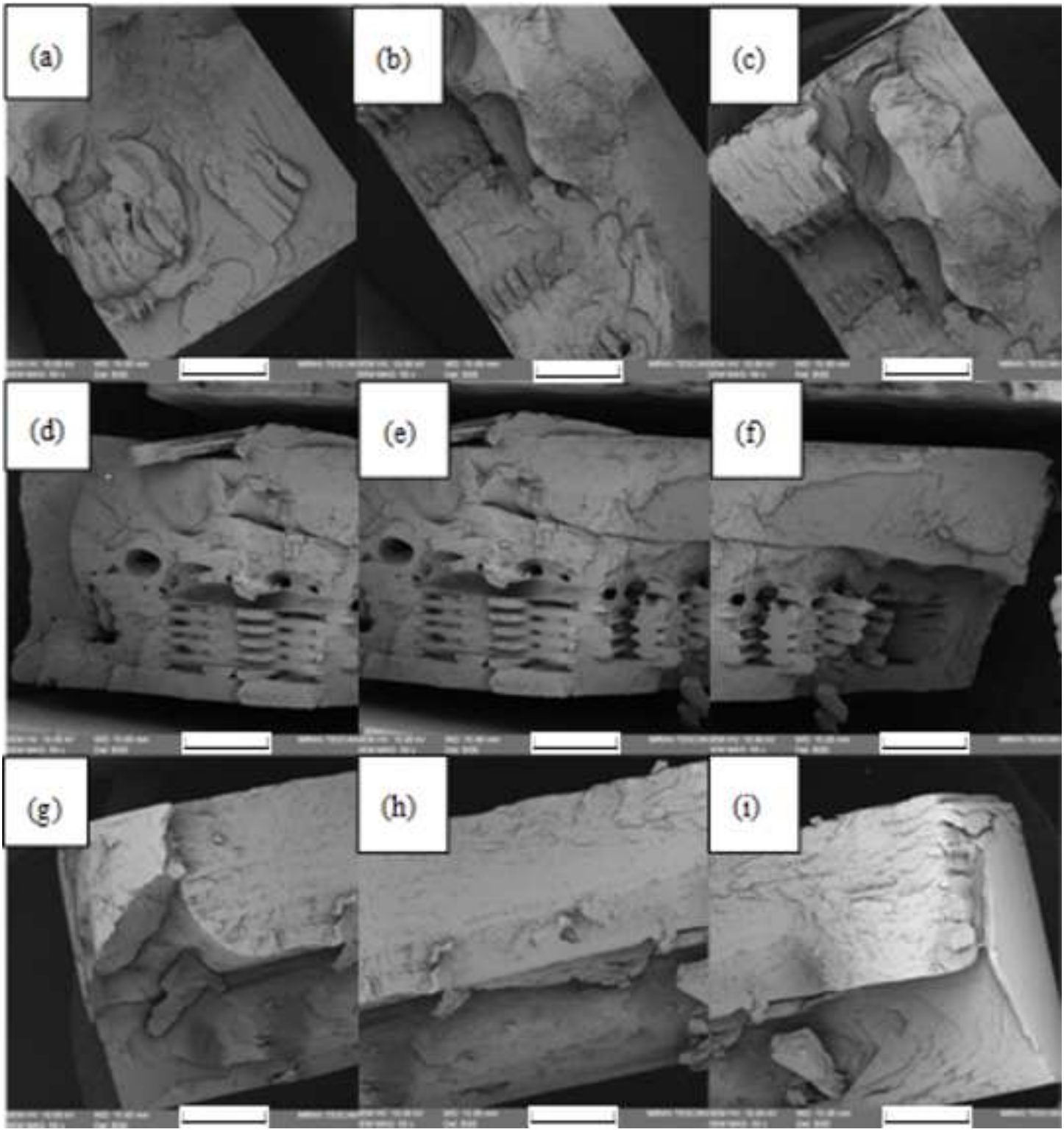

Figure 11 top

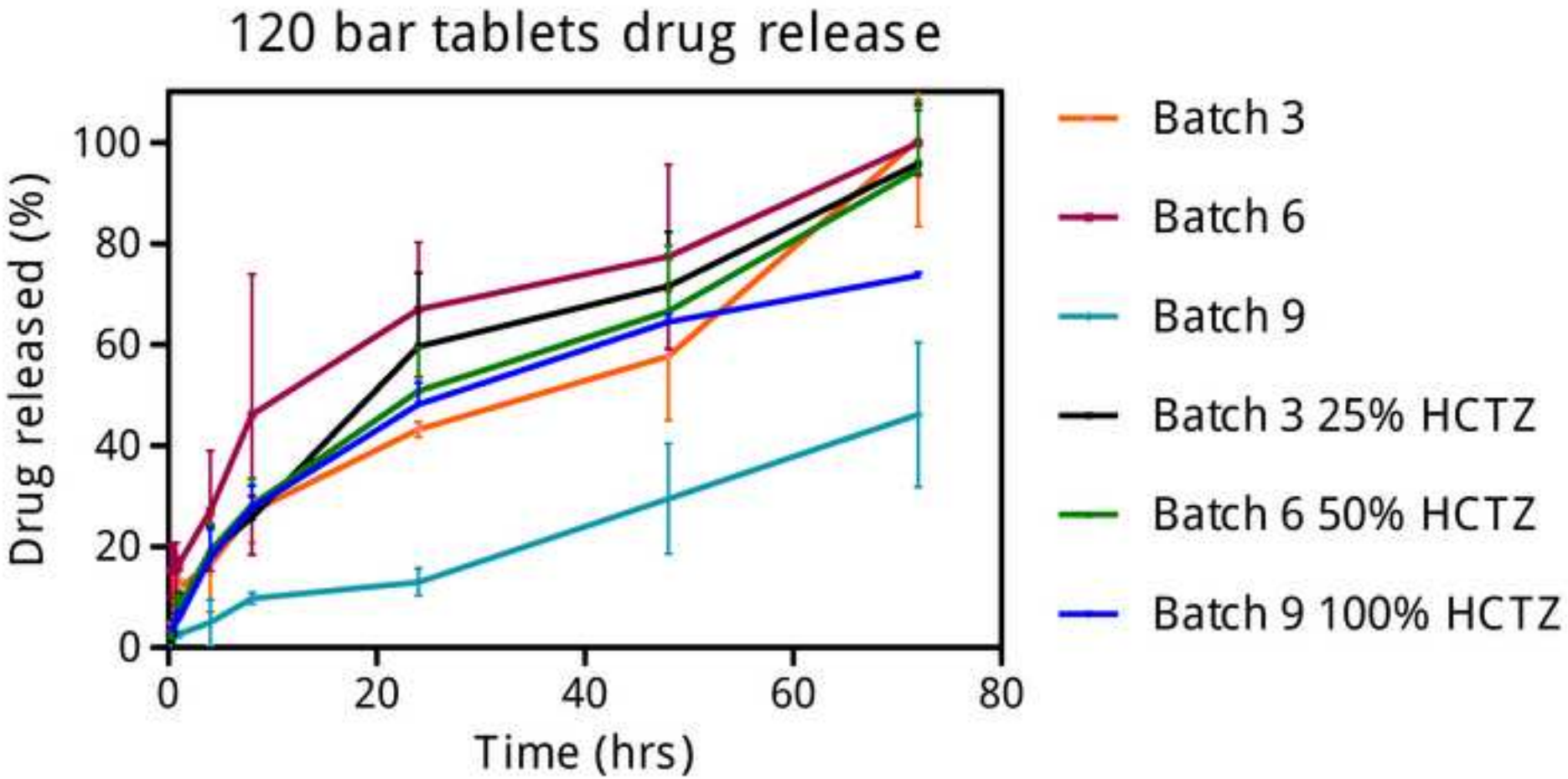

Figure 11 bottom